UNIMORE
UNIVERSITÀ DEGLI STUDI DI
MODENA E REGGIO EMILIA

UNIVERSITÀ DEGLI STUDI DI MODENA E REGGIO EMILIA

"Enzo Ferrari" Department of Engineering

Master of Science in Electronics Engineering - Industrial Automation (LM-29)

Design and Validation of a Printed Circuit Board Integrating a BGT60LTR11AIP mmWave CW Doppler Radar Sensor

Supervisor:
Ph.D. Pasquale Di Viesti
Co-Supervisor:
Prof. Giorgio Matteo Vitetta
Marco Mura, M.Sc

Candidate:
Antonio Corsini
195985

ACADEMIC YEAR 2025/2026

Abstract

In recent years, *millimeter-wave* (mmWave) radar technology has seen rapid adoption beyond its traditional military and automotive applications, establishing itself as a key solution in the fields of smart sensing, home automation, and non-invasive biomedical monitoring. Among the various architectures, *continuous-wave* (CW) radars offer an excellent balance between computational complexity, power consumption, and sensitivity in motion detection. This thesis presents the design, implementation, and validation of a custom embedded platform based on the Infineon BGT60LTR11AIP 60 GHz CW radar sensor of a custom embedded system to integrate and control the Infineon BGT60LTR11AIP CW radar sensor operating at 60 GHz. By utilizing the sensor's *Antenna-in-Package* (AiP) technology, a printed circuit board (PCB) was developed to reduce electromagnetic interference and ensure the integrity of the power and output signals. Concurrently, the corresponding software driver was developed for interfacing with the processing unit, enabling the correct configuration of the radar's operating parameters and the efficient acquisition of detection signals. The characterization results confirm the robustness of the hardware and validate the system for presence detection and micro-motion sensing. The development of this hardware-software platform lays the groundwork for future implementations focused on advanced signal processing algorithms, such as contactless monitoring of vital signs.

Contents

List of Figures

List of Tables

Introduction and Thesis Overview

The application of radar technology is rapidly expanding from traditional fields into small sensors for everyday use. In this context, CW mmWave radars offer a different trade-off from optical sensors such as LiDAR, particularly in terms of power consumption, privacy, and robustness to lighting conditions. While laser technologies perform well in high resolution 3D mapping, they are typically power demanding, sensitive to environmental conditions like light or dust, and raise significant privacy concerns. In contrast, a 60 GHz CW radar can be designed as a low-power sensor and is less privacy-invasive because it measures motion and phase variations rather than images. However, designing hardware for these millimeter wave frequencies presents a major practical challenge. At 60 GHz, routing signals on a standard PCB leads to high signal degradation and impedance problems. While specialized high-frequency materials can solve this issue, they significantly increase production costs, making them unsuitable for accessible prototyping and low-cost commercial applications. This thesis addresses this problem by presenting the hardware design and validation of a custom board built around the Infineon BGT60LTR11AIP CW radar and explaining the practical steps taken to move from theoretical radar principles to a physical prototype.

This thesis is organized into five chapters, each addressing a specific aspect of the custom radar embedded system:

- The first chapter provides a theoretical foundation by introducing the history of radar technology and the physical principles of the CW system, with a particular attention on the Doppler effect and the I/Q modulation architecture.

- The second chapter describes the core of the system, analyzing the internal architecture, radio frequency specifications and the operational modes of the BGT60LTR11AIP MMIC, justifying its selection for this project.

- The third chapter details the design and the implementation of the custom PCB. It describes the schematic of the board and the layout choices adopted to ensure proper board operation and signal integrity at 60 GHz.

- The fourth chapter details the practical hardware setup (including a logic level shifter and a

dielectric lens) and validates the system through I/Q signal analysis, phase unwrapping, and frequency estimation. The chapter then closes with a prototyping cost analysis.

- Finally, the conclusion summarizes the achieved results and outlines the potential for future industrial IoT applications.

1. Fundamental Principles and the State of the Art in Radar Systems

1.1 Introduction and Historical Overview

Radar, an acronym for Radio Detection and Ranging, has its roots in the late nineteenth and early twentieth centuries, beginning with Heinrich Hertz's experiments on the reflection of electromagnetic waves and the pioneering ideas of Nikola Tesla and Guglielmo Marconi. A major milestone was reached in 1904, when Christian Hülsmeyer patented the Telemobiloscope, the first operational device capable of detecting the presence of ships by utilizing the reflections of radio signals, and is often regarded as a precursor of modern radar. The true systematic development of the technology is owed to the pressing military needs of World War II for air defense and navigation, which led to the creation of long-range surveillance networks such as the British Chain Home system in 1937. In the years following the war, the introduction of solid-state electronics in the 1970s made it possible to build increasingly compact and reliable systems, while the advent of phased-array radar and digital signal processing (DSP) in the 1980s revolutionized tracking capabilities and electronic beam steering without the need for moving mechanical parts. Today, advances in semiconductor technology (such as CMOS and SiGe processes) have made it possible to integrate entire mmWave transceivers onto a single silicon chip. This dramatic reduction in cost and size has taken radar beyond the purely military context, transforming it into a pervasive and essential sensor for civil and industrial society [1].

1.2 Radar System Architecture and Applications

To understand the wide range of applications for modern radar, it is necessary to analyze its fundamental hardware structure. In its most basic configuration, a radar system consists of:

- A **local oscillator** that generates the radio frequency signal.
- A **transmitter (TX)** that amplifies and emits the wave via an antenna.
- A **receiver (RX)** that captures the echo reflected from surrounding targets.
- A **mixer** then combines the received signal with a copy of the transmitted signal to perform analog down conversion to baseband, making it ready to be digitized by an analog-to-digital converter (ADC) and processed by the digital signal processor (DSP).

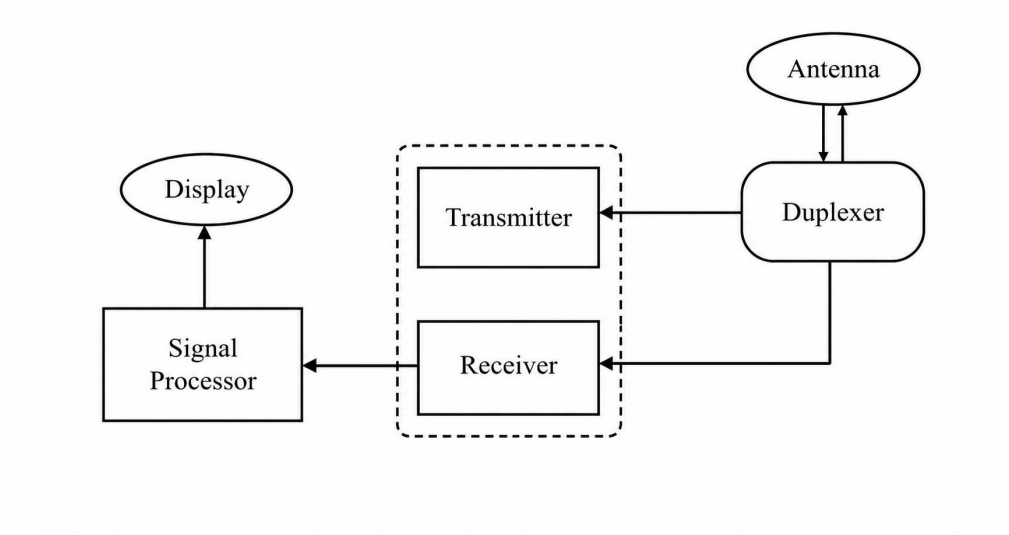

Figure 1.1: Radar Components Block Scheme.

Depending on the geometric arrangement of these components, radar systems are classified as follows:

- **Monostatic Radar**: where the transmitter and receiver are co-located or share the same antenna via a circulator. This is the standard configuration for most compact industrial and commercial sensors.

- **Bistatic/Multistatic Radars**: in which the transmit and receive antennas are spatially separated by a significant distance, requiring complex time and phase synchronization systems.

Furthermore, from the perspective of antenna hardware development, a distinction is made between *SISO*(Single-Input, Single-Output) systems, which use a single antenna for transmission and a single antenna for reception (ideal for simple, low-cost applications), and MIMO (Multiple-Input, Multiple-Output) systems, which use arrays of multiple antennas to electronically synthesize a large virtual antenna, drastically improving spatial resolution. There are also the *SIMO* (Single-Input, Multiple-output) and the *MISO* (Multiple-Input, Single-output). SIMO is a radar with a configuration composed of one transmitting antenna and multiple receiving antennas. The transmitting antenna emits an electromagnetic wave and when the signal bounces over a target, the returned echo is captured simultaneously by the array of received antennas. So long as the received antennas are physically separated, the returned wave hit them in different instants and with different phases. By processing these phase differences, the radar can estimate the **Direction of Arrival** (DoA), furthermore by combining the received signals, the quality is better in terms of signal to noise ratio. MISO is a radar where the configuration is made by a multiple transmitted antennas and a single received antenna. So different antennas emit signals toward the space, these signals may be identical with controlled phase shifts, or mutually orthogonal. The echo is captured by a single antenna.This type of radar is used for the *Beamforming*: coordinating the antennas is possible to concentrate the radar energy in a very narrow and precise direction, increasing the range, and for the *Spatial Diversity*: Since the signals hit the target from slightly different angles, the risk of echo cancellation due to the complex shape of the target itself is reduced. Thanks to this architectural flexibility and the ability to operate across various bands of the electromagnetic spectrum, radars find application in numerous key sectors:

- **Air Traffic Safety and Control**: Long-range systems for airspace monitoring and commercial route management.

- **Automotive and ADAS Systems**: Short-range and medium-range sensors integrated into vehicles for *adaptive cruise control*(ACC), automatic emergency braking, and blind-spot detection.

- **Infrastructure Surveillance and Security**: Perimeter monitoring of sensitive areas, intrusion detection, and structural monitoring of bridges or dams using interferometric techniques.
- **Smart Sensing and Industrial Automation**: Industrial sensors for calculating fluid levels in tanks, counting people inside rooms, and human machine interaction through gesture recognition.
- **Contactless Biomedical Monitoring**: One of the most promising frontiers, where radar is used to detect human physiological parameters (breathing and heart rate) without the patient having to wear electrodes or invasive devices, while ensuring full respect for privacy compared to optical cameras [2].

1.3 Fundamental Measured Quantities

A radar is an electronic system capable of detecting the presence of objects in the surrounding space, commonly referred to as targets, using radio-frequency electromagnetic waves. Its operation is based on a physical phenomenon called “backscattering", which occurs when a radar wave hits an object and part of the wave’s energy is reflected back toward the radar. This reflected energy

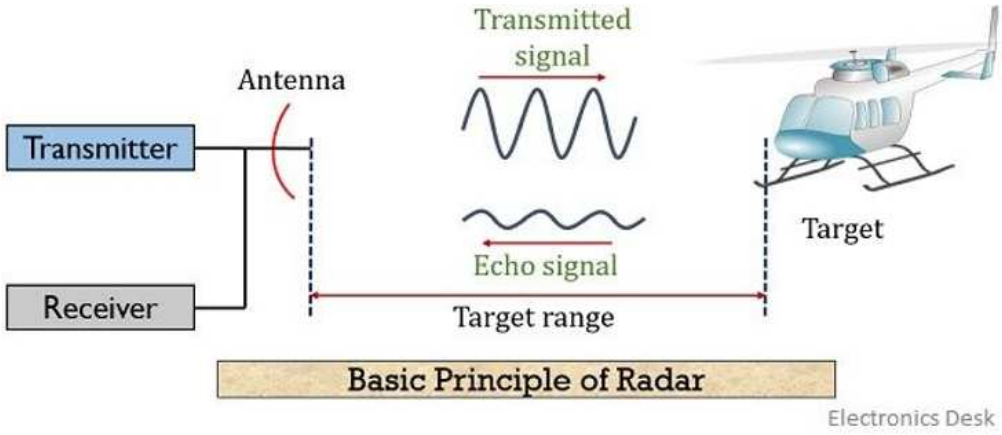

Figure 1.2: Work Principle of Radar.

can be detected by the receiver antenna of radar and used to determine the position, the velocity and characteristics of the object that caused the reflection. Regardless of the specific application context or the chosen hardware architecture, the interaction of the radar signal with the surrounding environment is governed by well defined physical laws. The primary objective of the data processing block is to extract 3 kinematic and spatial parameters of the target: **range**, **radial velocity**, and **angle of arrival**. The measurement of the angle of arrival is possible only in the case of arrays of antennas [3].

1. **Distance (Range, R)**: The distance estimate is based on calculating the round trip delay time τ that the electromagnetic wave takes to travel from the sensor to the target and back. Knowing the speed of light in the medium c, the distance is determined by the relationship:

$$R = \frac{c * \tau}{2} \tag{1.1}$$

2. **Velocity (v)**: The target's velocity along the radar line of sight (radial velocity) is derived by measuring the frequency shift of the reflected wave with respect to the transmitted wave; this is a physical phenomenon known as the Doppler effect f_D.

3. **Angle of Arrival (Θ)**: The angular information (both in azimuth and elevation) is calculated using the phase difference or time delay with which the target's echo hits the various receiving antennas arranged geometrically in an array.

The waveform emitted by the transmitter toward the target returns to the receiver as an echo. The return radiation can be detected by one or more receiving antennas with a certain delay, equal to twice the antenna-target propagation time: knowing the propagation speed of the electromagnetic wave in the medium in question, it is therefore possible to determine the target's distance and its angular position relative to the reference system if multiple antennas are used. With reference to the classic case of a simple radar consisting of a transmitter and a receiver, the fundamental radar equation, namely the relationship between the incident power density at the target S_T, transmitted power P_T, and the radar-target distance R, is:

$$S_T = \frac{P_T G_T}{4\pi R^2} \quad [W/m^2] \tag{1.2}$$

where G_T is the transmitted gain. Furthermore, A_e is defined as the Effective Area of the receiving antenna, as

$$A_e = \frac{G_R \lambda^2}{4\pi} \quad [m^2] \tag{1.3}$$

where G_R is the gain of the receiving antenna and λ is the wavelength of the signal. The physical feasibility of this detection and the maximum range of the sensor are described mathematically by the radar equation. For a monostatic system operating in free space, the power of the echo signal returning to the receiver ($P(r)$) is related to the system parameters by the following formula:

$$P(r) = \frac{P_T G_T G_r \lambda^2 \sigma}{(4\pi)^3 R^4} \tag{1.4}$$

assuming matched polarization and free-space propagation. σ is known as the *Radar Cross Section* (RCS), a parameter that measures the target's ability to reflect the incident wave. The higher the RCS, the more likely it is that the object will be correctly detected by the radar and P_T is the transmitted power, G_T and G_R are the transmit and receive antenna gains, respectively, λ is the

wavelength of the carrier signal, and σ represents the target's radar cross section, i.e., its intrinsic ability to reflect radio waves. The presence of the term R^4 in the denominator highlights how the useful signal undergoes extremely severe geometric attenuation, making printed circuit board (PCB) design and the noise immunity of the analog front-end critical factors for the system's success. Using this equation, it is possible to derive parameters such as P_T or P_R given the minimum value of P_R, based on the receiver's sensitivity. It is important to note that the received power is proportional to the square of the signal's wavelength.

1.4 Classification Based on Waveforms

The way in which a radar modulates electromagnetic energy over time defines its waveform and determines which of the fundamental parameters (distance, velocity, or angle) can be extracted, as well as the accuracy and resolution of the measurement itself. The main modulation strategies fall into four broad categories:

- **Continuous Wave (CW)**: Pure continuous wave radars do not use any modulation of the transmitted signal, which consists of a constant sinusoidal waveform at a fixed frequency. The absence of frequency variations or time pulses means that the signal has no time markers; consequently, a CW radar is unable to measure the time of flight τ, making it impossible to determine the target's absolute distance. However, as will be seen in detail, the continuous wave proves to be the most efficient, simple, and energy efficient tool for the pure measurement of velocity and micro-oscillations [4].

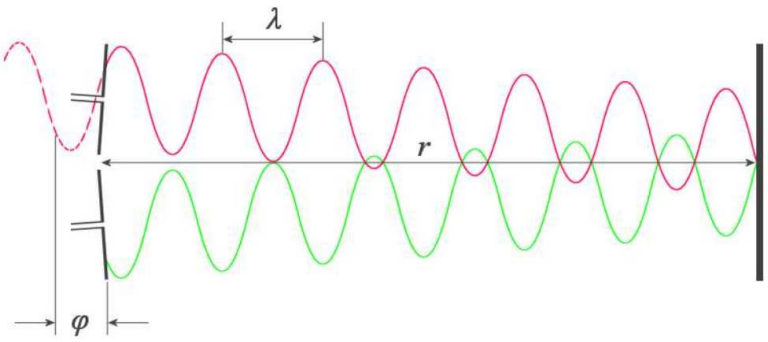

Figure 1.3: CW radar signal.

- **Impulse-Radio Ultra-Wideband (IR-UWB)**:This technology uses extremely short radio pulses (on the order of picoseconds or nanoseconds). Due to the properties of the Fourier transform, such a time limited pulse occupies an immense spectral bandwidth (hence the term Ultra-Wideband). The reflected pulses are sampled and processed using matched filters; the high bandwidth guarantees millimeter level spatial resolution in distance measurement, making them ideal for short range applications [5].

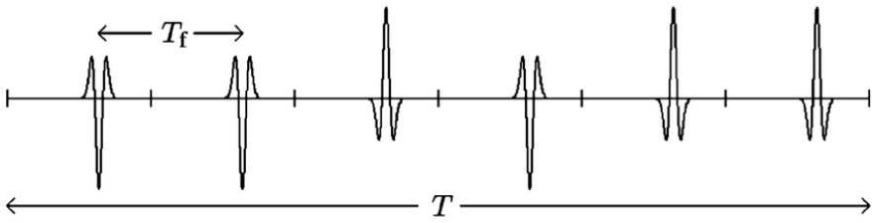

Figure 1.4: An Impulse Radio UWB signal containing short pulses with a low duty cycle

- **Frequency-Modulated Continuous-Wave (FMCW)**:Unlike UWB, FMCW radars emit a continuous signal whose frequency varies linearly over time (typically a sawtooth or triangular ramp, called a chirp). By mixing the received signal with the transmitted signal, a beat frequency (f(b)) proportional to the time of flight is obtained; the application of a two-dimensional Fast Fourier Transform (2D-FFT) allows for the simultaneous and separate mapping of the distance and velocity of multiple targets.

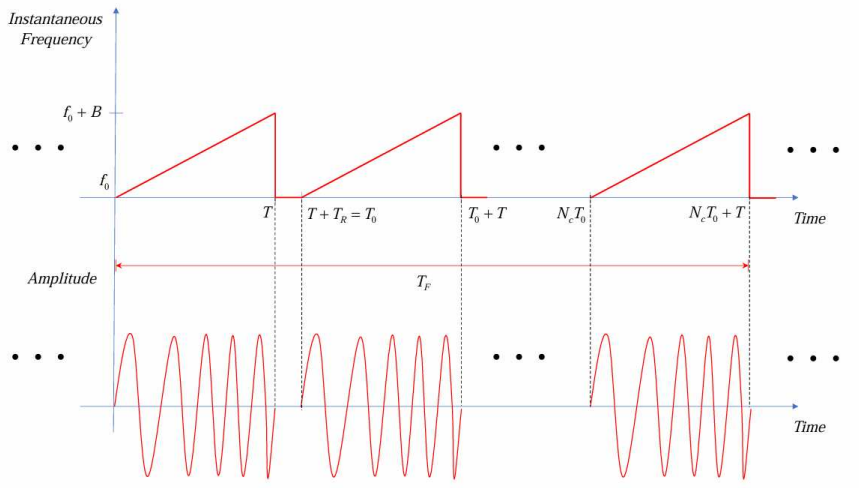

Figure 1.5: FMCW signal

- **Stepped-Frequency Continuous-Wave (SFCW)**:Stepped-Frequency Continuous-Wave (SFCW): In this architecture, the transmitter sends an ordered sequence of sinusoidal tones at a fixed frequency, incrementing the frequency value in discrete steps at each interval. The frequency response of the environment is sampled in the frequency domain, and the distance profile is subsequently reconstructed by applying the Inverse Fast Fourier Transform (IFFT).

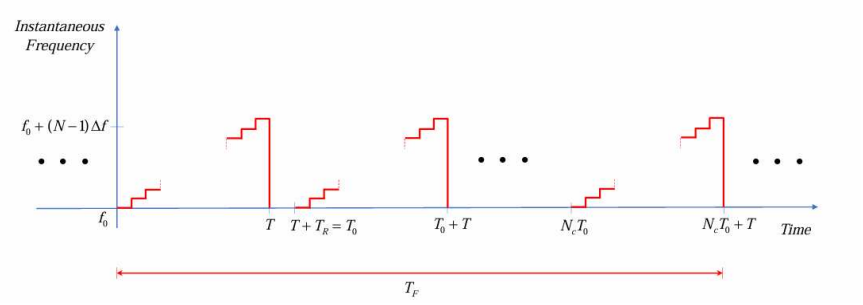

Figure 1.6: Time-frequency profile of an SFCW radar signal

1.5 Continuous-Wave (CW) Radar and the Doppler Effect

Unlike pulsed radars, which emit short pulses of energy and then listen for the echo to calculate the time of flight (and thus the distance), a CW radar simultaneously transmits and receives a continuous electromagnetic wave. Its primary purpose is not to measure static distance, but to exploit the Doppler effect. When the transmitted wave strikes a moving object, the reflected wave undergoes a frequency shift:

- If the target is moving closer, the received frequency increases.
- If the target is moving away, the received frequency decreases.

Fig. 1.7 illustrates how the radar front-end converts the Doppler frequency shift into baseband I/Q signals that can be digitized and processed.

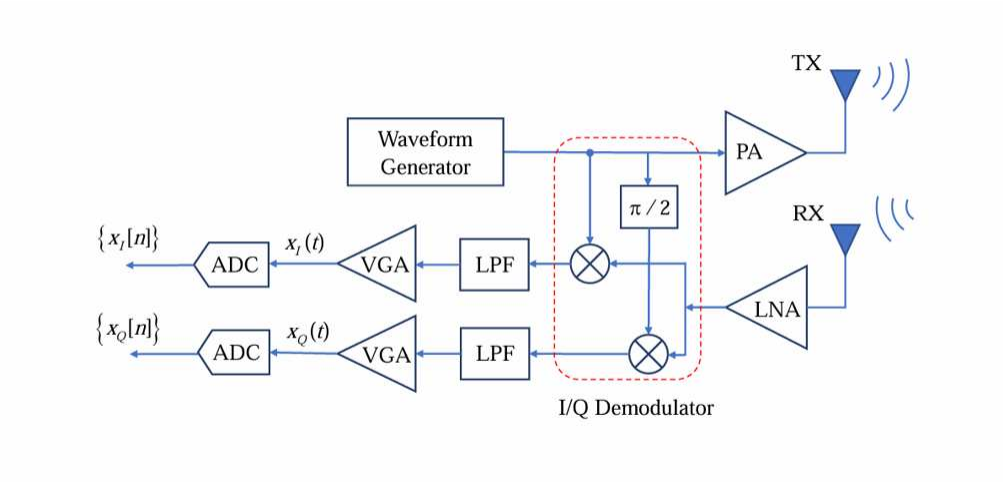

Figure 1.7: Radar Block scheme.

The system can be described through the following functional blocks:

1. **Transmission Section (TX – top right)** Waveform Generator: This is the local oscillator. It generates a continuous microwave signal at a fixed frequency (e.g., 24 GHz or 60 GHz).
2. **PA (Power Amplifier):** Amplifies the generated signal to provide it with sufficient power before sending it to the antenna.
3. **TX Antenna**: Radiates the electromagnetic wave into the surrounding environment.

4. **RX Antenna (RX – bottom right)**: Captures the echo reflected from targets (which will contain the Doppler frequency shift if the target is moving).

5. **LNA (Low Noise Amplifier):** The return signal is extremely weak. The low noise amplifier has the delicate task of amplifying it without adding too much electronic "noise," which would otherwise mask the useful information.

6. **I/Q Demodulator (Red dotted box)**: To extract the Doppler frequency, the received signal is compared (mixed) with an exact copy of the signal originally transmitted. The circles marked with an "X" are the mixers. They multiply the transmitted signal by the received signal. Why are there two branches? If we had only one mixer, we would get a beat that tells us how fast the object is moving, but we wouldn't know if it's approaching or receding. To solve this problem, the original signal is split: one branch goes to the first mixer to create the I (In-phase) channel, while the other is phase-shifted by 90 degrees (represented by the $\pi/2$ block) before going to the second mixer to create the Q (Quadrature) channel. By analyzing which of the two signals (I or Q) arrives first, the radar unambiguously determines the direction of motion [6].

7. **Baseband Conditioning and Digitization (Left)** The signals output from the mixers are now low-frequency (baseband) and follow the twin I and Q paths:

    - LPF (Low Pass Filter): Filters out the unwanted high frequencies generated by the multiplication in the mixer, allowing only the clean Doppler signal $x_I(t)$ and $x_Q(t)$ to pass.
    - VGA (Variable Gain Amplifier): Amplifies the filtered analog signals so that they have the perfect amplitude for the next converter.
    - ADC (Analog-to-Digital Converter):The final step. Converts the continuous analog waves into discrete digital samples, represented as the sequences $x_I[n]$ and $x_Q[n]$.

The signal emitted by the transmitter can be modeled as

$$s_{TX}(t) = A_{TX}\cos(2\pi f_C t + \phi), \tag{1.5}$$

where f_C is the frequency of the radio carrier and ϕ is the initial phase. When the wave encounters a target located at a distance $R(t)$ moving with a constant radial velocity v, the wave undergoes reflection and returns to the sensor, accumulating a variable time delay

$$\tau = \frac{2R}{c} \tag{1.6}$$

The signal captured by the receiving antenna is therefore

$$s_{RX}(t) = A_{RX}\cos(2\pi f_C(t - \tau(t)) + \phi) = A_{RX}\cos\left(2\pi f_C t - \frac{4\pi f_C R(t)}{c} + \phi\right) \tag{1.7}$$

Since the target is moving, its distance can be expressed as $R(t) = R_0 - vt$,where R_0 is the position at the initial instant. Substituting this expression into the phase term of the received signal yields

$$s_{RX}(t) = A_{RX}\cos\left(2\pi\left(f_c + \frac{2vf_c}{c}\right)t - \frac{4\pi f_C R_0}{c} + \phi\right) \tag{1.8}$$

The formula highlights the frequency shift experienced by the signal, defining the Doppler frequency f_D as:

$$f_D = \frac{2vf_c}{c} = \frac{2v}{\lambda} \tag{1.9}$$

with a clear sign convention for approaching/receding targets. Through the analog mixing stage (down conversion), the ultra-high-frequency carrier signal f_c is removed, and the output from the mixer is a base band signal whose frequency corresponds exactly to f_D. By measuring the spectrum of this signal, it is possible to instantly determine the target's velocity. However, a single mixer would generate a real signal of the form $cos(2\pi\ f_D t)$, making it impossible to distinguish whether the Doppler frequency is positive (approaching target) or negative (receding target). The in-phase $I(t)$ and the quadrature component $Q(t)$ are:

$$I(t) = I_0\cos(2\pi f_D t + \Psi) \tag{1.10}$$

$$Q(t) = Q_0\sin(2\pi f_D t + \Psi) \tag{1.11}$$

Analysis in the complex-signal domain, $S(t) = I(t) + jQ(t)$, preserves the sign of the Doppler frequency and enables motion-direction estimation.

1.6 From Theory to Practice: The 60 GHz Challenges and Introduction to the MMIC

Up to this point, we have explored the theoretical basics of CW radars. We have seen how, by using the quadrature (I/Q) architecture, it is possible to extract highly precise information about a target's movement and direction. However, moving from these mathematical models to a real, physical device introduces a major engineering challenge, mostly related to the operating frequency. To achieve the sensitivity needed to detect micro movements, modern radars often work in the millimeter-wave (mmWave) band, for example at 60 GHz. At this frequency, the wavelength is only about 5 millimeters. At these extreme frequencies, building a traditional radar system using discrete components is a very hard task. Routing 60 GHz signals on a standard printed circuit board (PCB) to external antennas would cause huge signal losses. It would also require very expensive special materials and microscopic manufacturing precision. To overcome these physical and economic barriers, the semiconductor industry has developed highly integrated single chip solutions (MMIC - Monolithic Microwave Integrated Circuits). One example of this technological evolution, which is also the core of this thesis work, is the Infineon BGT60LTR11AIP sensor. This component includes the entire radar architecture described in the previous paragraphs: the waveform generator, the mixers, and the I/Q amplification chain. Even more importantly, it integrates the transmitting and receiving antennas directly inside the chip. In this way, the complex 60 GHz dynamics stay confined and protected inside the silicon. The chip only outputs low-frequency signals that are ready to be processed. The Second Chapter will be entirely dedicated to an in-depth analysis of this sensor. We will explore its internal hardware architecture, its radio frequency specifications, and its communication interfaces. This will help us fully understand how this component translates the complex principles of radar physics into a practical tool, ready to be integrated into embedded systems.

2. The Infineon BGT60LTR11AIP Radar Sensor

2.1 Introduction and Component Selection

The evolution of radar systems for short-range applications has accelerated dramatically in recent years, driven by the need to integrate smart sensors into devices with stringent constraints on space, cost, and power consumption. While in the past, radar systems operating at mmWave frequencies required architectures with discrete components, today a common solution is the use of Monolithic Microwave Integrated Circuits (MMICs).

In the context of this thesis, the component chosen as the heart of the system is the Infineon BGT60LTR11AIP sensor. Specifically, this is a CW Doppler radar operating in the 60 GHz ISM (Industrial, Scientific, and Medical) band. The choice of a CW architecture for this specific chip is due to its efficiency. Unlike the complex FMCW radars widely used in the automotive industry, which require a lot of power to generate frequency modulation ramps and calculate heavy mathematical Fourier transforms (FFTs), the BGT60LTR11AIP transmits a single unmodulated continuous tone. This allows it to focus exclusively on the Doppler effect in order to measure speed and micro-movements while drastically reducing computational load and hardware complexity. The choice of this MMIC for the project was driven by three key engineering reasons:

- **Extremely high level of integration**: The chip measures just 3.3 × 6.7 × 0.56 mm and incorporates not only the entire CW radio frequency front-end, but also the digital control logic and the antennas themselves.
- **Operational flexibility**: The sensor is designed to function both as a stand-alone detector and as an advanced peripheral device controllable via a digital bus (SPI), making it perfectly suited for the development of custom software drivers.
- **Ultra-low power consumption**: Thanks to the simple nature of the continuous wave combined with duty cycling techniques, the component is able to operate with an average power consumption of less than 2 mW.

2.2 Radio Frequency Specifications and Antenna-in-Package (AiP) Technology

One of the most critical aspects of hardware design for circuits operating at 60 GHz is managing how the radio signals travel on the circuit board (PCB). At these frequencies, dielectric losses and impedance mismatches caused by copper traces severely degrade radiated power and sensitivity. To overcome this problem, high-frequency laminates would need to be used, which increase production costs tenfold. The BGT60LTR11AIP resolves this bottleneck by adopting Antenna-in-Package (AiP) technology. Infineon has integrated a set of antennas, one for transmission and one for reception, directly into the silicon package substrate. The patch-type antennas have a gain of approximately 6 dBi and offer a very wide field of view (FOV), with a half-power beam width (HPBW) of about 80 degrees, which is optimal for volumetric monitoring. From a PCB design point of view (which will be seen in Chapter 3), the use of AiP confines all 60 GHz propagation within the chip. The pins exposed by the component carry only power lines and low-frequency baseband analog or digital signals [7].

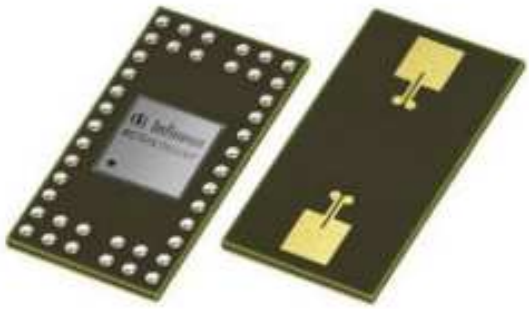

Figure 2.1: BGT60LTR11AIP chip Radar.

2.3 Internal Architecture and Block Diagram

Looking at the internal setup of the MMIC chip shows that the BGT60LTR11AIP is a mixed system that physically implements the mathematical models discussed previously.

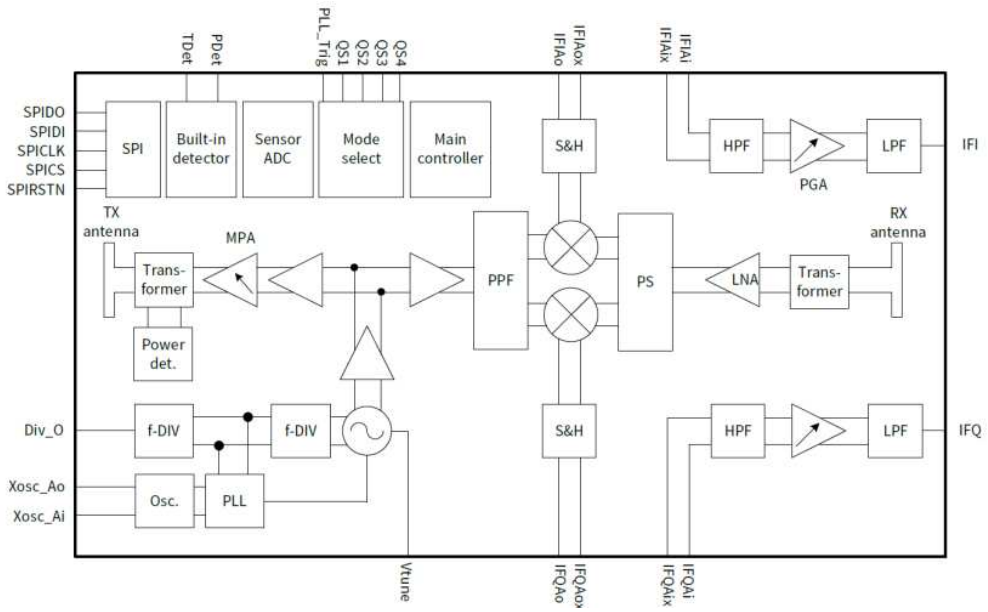

Figure 2.2: Infineon chip internal scheme. [8]

The main blocks that form the core of the sensor are:

- **CW Generator (VCO and PLL):** The 60 GHz steady radio wave is created by a voltage-controlled oscillator (VCO) with very low phase noise, held steady by a phase-locked loop (PLL) control block. Since this is a CW radar, the PLL keeps the frequency strictly locked onto a single tone in the ISM band without making any frequency changes.
- **Power Amplifier (PA) and TX**: The continuous wave is fed to the power amplifier that drives the transmit antenna. An integrated power detector monitors the actual output power, allowing the software to scale the radiated power.

- **Low Noise Amplifier (LNA):** On the receive path, the weak CW signal reflected by the targets (affected by Doppler shift) is captured by the RX antenna and amplified by the LNA, minimizing the noise figure.
- **I/Q Demodulator**: The received signal is split and multiplied (via two mixers) by the original continuous wave generated by the VCO. To preserve the information regarding the direction of motion, the mixing is performed using two carriers that are 90 degrees out of phase, thereby precisely extracting the I component and the Q component.
- **Baseband Chain**:The I and Q signals output from the mixers pass through low-pass filters to eliminate 60 GHz residuals and are amplified by analog Variable Gain Amplifiers (VGAs) before being routed to the output pins.

2.4 Operating Modes: Autonomous Mode vs. SPI Mode

The main special feature of the BGT60LTR11AIP is its ability to use two different operating modes. The chip can be initialized in two diametrically opposed modes: **Autonomous Mode** and **SPI Controller Mode**.

2.4.1 Autonomous Mode

In this mode, the sensor operates completely independently as a plug-and-play device. Once powered, the integrated digital state machine checks the analog I/Q signals using internal comparators and manages the detection logic. The sensor provides the output directly on two digital output pins:

- TDet (Target Detect): Goes high when a moving target is detected.
- PDir (Phase Direction): When TDet is high, it indicates the target's direction (high for approaching, low for receding)

The absence of a microcontroller requires a hardware method to configure and set parameters such as sensitivity or hold time. Infineon solves this problem by using the Quad State (QS) pins (QS1, QS2, QS3, QS4), which are able to recognize four different electrical states (Ground, VDD, Open, or connection via a resistor). By combining these pins on the PCB, we can select from

multiple threshold levels and hold times. Despite this mode offers extreme circuit simplicity, it has limits because the configurations are fixed and the raw CW I/Q data cannot be analyzed by software [7].

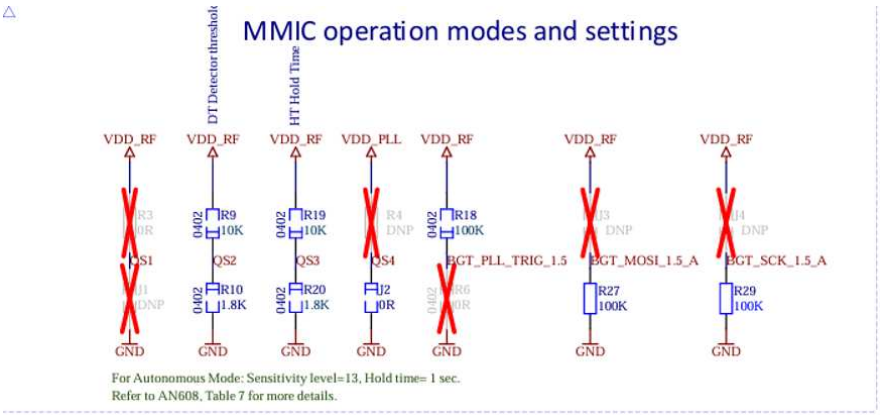

Figure 2.3: Autonomous mode schematic for BGT60LTR11AIP.

This is the quad states configuration for autonomous mode.

2.4.2 SPI Mode (Serial Peripheral Interface)

To unlock the full potential of the CW radar, access dynamic configurations, and enable fine phase extraction (e.g., for monitoring vital parameters as previously described), it is necessary to use SPI mode. This is the mode implemented in this thesis. In SPI mode, the BGT60LTR11AIP is connected to a microcontroller unit (MCU) chip. Through the SPI communication lines, the software driver can read and write to the MMIC's internal registers. In SPI mode, the radar configuration is controlled through internal registers, while the BBI/BBQ analog outputs are sampled by the external ADC. The data sampled by the ADC are read by an external MCU through the SPI. This brings many benefits:

- **Raw Data Reading**: The pure analog I and Q signals are sent out directly to the MCU's analog-to-digital readers (ADCs), allowing the software to use math formulas to detect tiny, millimeter-sized movements.
- **Runtime Reconfiguration**: Detection thresholds, gains (VGA), and timing parameters can be adjusted in real time based on the environmental context.

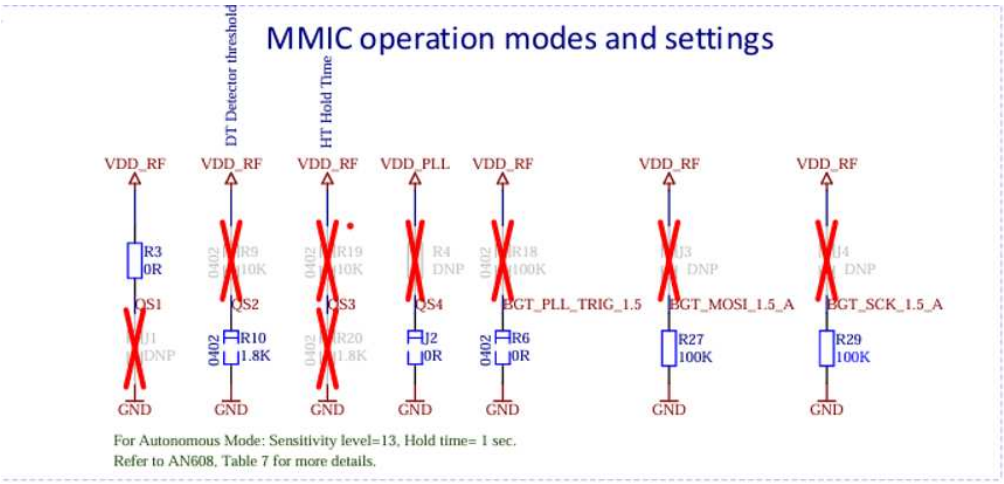

Figure 2.4: SPI mode schematic for BGT60LTR11AIP.

This is the quad states configuration in the SPI Mode.

2.5 Pinout and Hardware Interfaces

Placing the BGT60LTR11AIP into the circuit schematic requires a careful analysis of its pinout and the separation of signal paths. The chip is built in an extremely compact package with connection pads on the bottom, which makes correct assignment and routing of traces on the PCB crucial. To ensure maximum signal integrity and prevent internal interference (crosstalk), the sensor's pins are logically and physically grouped into four functional domains:

- Power supply
- Digital control
- Analog outputs
- Hardware configuration

2.5.1 Power Supply Management (Power Supply Domain)

Due to the coexistence of highly sensitive radio-frequency circuits and high-speed digital logic, the MMIC requires strictly separated power supply paths. This prevents digital switching noise from coupling into the receive chain. The main power supply pins are divided into:

- **VDD_RF (1.5 V)**: This is the most critical connection in the entire system. It supplies the Voltage Controlled Oscillator, the PLL, and all 60 GHz circuitry (LNA and PA). This domain must be powered via a low-noise, low-dropout (LDO) linear regulator . The printed circuit board layout requires a dense network of decoupling capacitors (in the order of pF and nF) positioned as close as possible to the silicon pads, in order to filter high-frequency transients and provide ultra-low-impedance ground return paths.

- **VDD_BB (1.5 V)**: This line powers the baseband analog chain, which includes the filters and Variable Gain Amplifiers (VGAs). This voltage must also be extremely clean: any noise (ripple) on this line would directly overlap the weak Doppler signals (in the millivolt range), degrading the overall signal-to-noise ratio (SNR).

- **VDD_DIG** : Powers the logic parts of the SPI interface, the internal controller, and the digital input/output pins.

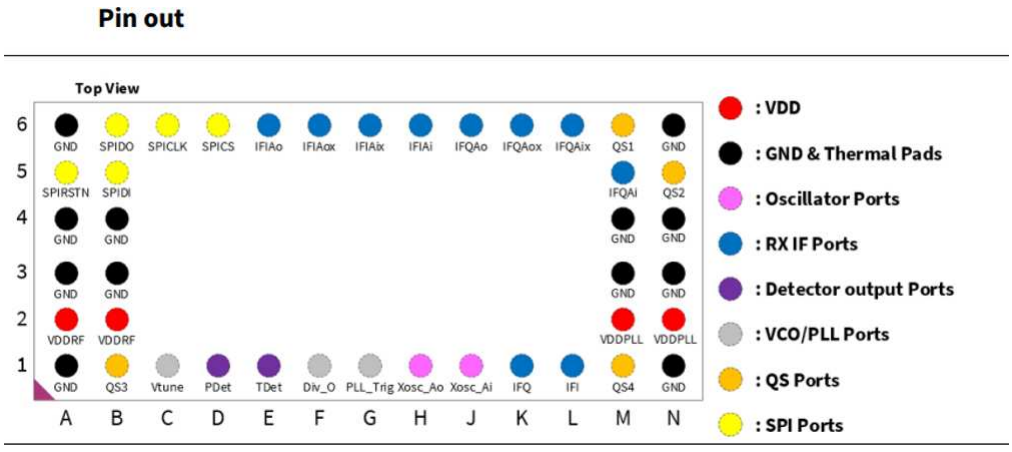

[8]

Figure 2.5: BGT60LTR11AIP Pin configuration.

2.5.2 Digital Interface and Control (SPI and I/O)

The operational control of the BGT60LTR11AIP, especially in advanced mode, is handled by a set of digital pins that perform both synchronous communication functions and asynchronous interrupt functions:

- **4-wire SPI bus**: This includes the standard signals CSN (Chip Select Not, active-low), CLK (Synchronization Clock), MOSI (Master Out Slave In), and MISO (Master In Slave Out). This interface serves as the primary communication channel between the software driver (implemented in the microcontroller) and the radar's internal registers.
- **Interrupt Pins (TDet and PDir)**: In addition to the data bus, the chip exposes two status pins. TDet (Target Detect) acts as a hardware interrupt line, going high as soon as the logic detects movement. PDir (Phase Direction), on the other hand, encodes the direction of motion (approaching or receding). In a low-power software architecture, these pins are essential: they allow the MCU to remain in Deep Sleep mode and wake up (via an external interrupt) only when the radar signals a relevant event.

2.5.3 Baseband Analog Outputs

For advanced signal processing, like the phase-based processing for monitoring micro-movements, the designer must be able to access the demodulated continuous wave. To do this, the chip provides: BBI (Baseband In-Phase) and BBQ (Baseband Quadrature): These two pins carry the analog, continuous, and pre-amplified copies of the I and Q signals output from the mixers. Since these are very low-frequency analog signals with low amplitude, their routing on the board to the microcontroller's ADCs requires careful shielding to prevent capacitive coupling with nearby clock signals.

2.5.4 Hardware Configuration Domain (Quad States)

The QS (Quad State) pins deserve a special mention. Their main job is to lock in the settings during Standalone mode, the way they are wired when the chip first turns on (boot phase) is highly important. Depending on how these QS pins are wired on the board (to ground, to VDD, left

unconnected, or wired through resistors), the chip decides which mode to start in, such as forcing a start into SPI mode. Getting these connections right in the schematic is a basic rule handled during the hardware design phase.

2.6 Power Consumption and Duty Cycling (Pulsed CW Mode)

A final, highly important engineering detail of the BGT60LTR11AIP is its ability to keep its average power use under 2 milliwatts. Leaving a 60 GHz oscillator running all the time would use too much power for battery-powered items (like IoT). To beat this limit without losing the benefits of the continuous-wave design, the chip works in Pulsed CW mode (also called Pulsed Doppler or Duty Cycling). Instead of broadcasting all the time, the internal power controller turns on the radio parts for just a tiny fraction of time (called Active Time). After that, it shuts down the radio front-end and goes into a deep sleep state. This steady cycle of turning on and off is controlled by a setting called Pulse Repetition Time (PRT), which sets the time gap between two checks (for example, every 0.5 ms or 5 ms). During the very brief window when the radar is awake, it sends out the wave, catches the Doppler reflection through its mixers, updates the BBI/BBQ pins and internal memory slots, and then immediately goes back to Deep Sleep.

3. Hardware and PCB Design

3.1 Introduction

This chapter describes in detail the hardware design phases for the creation of the custom board dedicated to integrating the Infineon BGT60LTR11AIP radar sensor. The primary objective of the design was to provide an optimal operating environment for the radar chip, ensuring an ultra-low-noise power supply, proper conditioning of the analog output signals, and a robust interface to the host microcontroller. The design was carried out using the KiCad EDA environment, dividing the work into two main phases: schematic capture and subsequent PCB layout. To maintain a clear and modular organization, the schematic was divided into hierarchical sheets, separating the control logic and the sensor, the power supply network, and the analog signal filtering networks. To ensure system reliability and the integrity of the ultra-high-frequency signals (60 GHz), each component was selected according to precise technical constraints and industry recommendations.

3.2 Electrical Schematic Design

3.2.1 Radar Core, Interfacing, and Clock Generation

The heart of the system is the BGT60LTR11AIP IC (Sheet 1/3). Interfacing with the external control logic is achieved via a 32-pin connector (J1), through which the SPI bus signals (MISO, MOSI, SCK, CS) for the configuration of the internal registers, the control lines, and the baseband signals are routed. Component Analysis:

- **BGT60LTR11AIP MMIC Sensor (IC1)**: The choice of this specific integrated circuit is driven by its AiP architecture. Operating at 60 GHz would require the use of expensive RF substrates and antenna routing that is extremely critical in terms of geometric tolerances. Integrating the antennas directly into the chip package eliminates insertion losses and mismatch

on the PCB, allowing the use of a standard, more economical FR4 substrate. Additionally, the IC integrates a motion detector, reducing the computational load on the host microcontroller.

- **FH3840024Z Crystal Oscillator (Y1)**: The radar operates by converting a stable reference frequency via an internal PLL synthesizer. The BGT60LTR11AIP datasheet strictly requires a clock frequency of 38.4 MHz with stringent thermal stability and low phase noise (jitter) requirements. This specific crystal ensures that the internal VCO (Voltage Controlled Oscillator) remains locked to the correct carrier frequency, minimizing frequency drifts that would compromise the Doppler measurement [9].

- **Load Capacitors C1 and C2**: These components are essential for ensuring that the Y1 crystal oscillates at its nominal parallel resonance frequency. The value of 12 pF was calculated using the formula for the load capacitance as seen by the crystal:

$$C_L = \frac{C_1 * C_2}{C_1 + C_2} + C_{stray} \tag{3.1}$$

Given a stray capacitance of the traces C_{stray} estimated to be between 1 pF and 2 pF, two symmetrical 12 pF capacitors provide an effective load capacitance of approximately 7–8 pF, which is perfectly aligned with the electrical specifications of the crystal used.

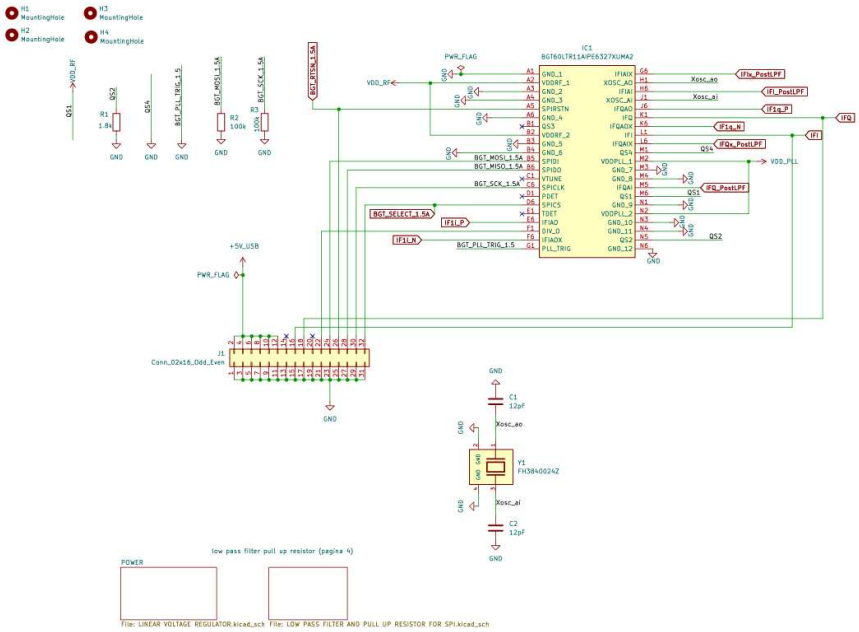

Figure 3.1: Sheet (1/3). BGT60LTR11AIP Schematic and Oscillator.

3.2.2 Power Supply (Power Management)

The performance of a high-frequency radar sensor is highly dependent on the quality of the power supply voltage. Noise on the lines can directly modulate the VCO, generating ghost targets or increasing flicker noise, thereby reducing the system's sensitivity. A dedicated network has been implemented in Sheet 2/3. Component Analysis:

- **Inductor L1 (10 µH) and Input Stage**: Located on the 5V input line (e.g., from USB), the inductor shields the board from differential-mode noise and the high ripple typical of switching power supplies. Together with the input capacitor bank (C3, C4, C5, C6), it forms an LC low-pass filter with a very low cutoff frequency.

- **LDO LDLN025M15R (U1) - 1.5V Line**: It was chosen for its low-noise performace: ultra-low output noise (6.5 microVrms) and very high PSRR (Power Supply Rejection Ratio 80dB). This linear regulator feeds the radar critical RF and PLL blocks [10].

- **LDO LDLN050PU33R (U2) - 3V3 line**: Dedicated to powering the digital section and control logic. It ensures that logic transitions and signals on the SPI bus do not introduce ground bounce or ripple on the system's analog line [11].

- **BLM18KG121TH1D Ferrite Beads (FB1, FB2, FB3)**: They have a characteristic impedance of 120Ω at 100 MHz and low DC resistance. Included to form π filters, they block high-frequency noise (EMI) and prevent digital switching noise from propagating to the analog power supply.

- **Decoupling Network (10 µF and 100 nF)**: A parallel combination of 10 μF and 100 nF ceramic capacitors is connected to each power supply line to reduce the impedance of the power distribution network (PDN). The 10μF capacitor acts as a sink for low-frequency transients, while the 100 nF capacitor attenuates high-frequency noise spikes.

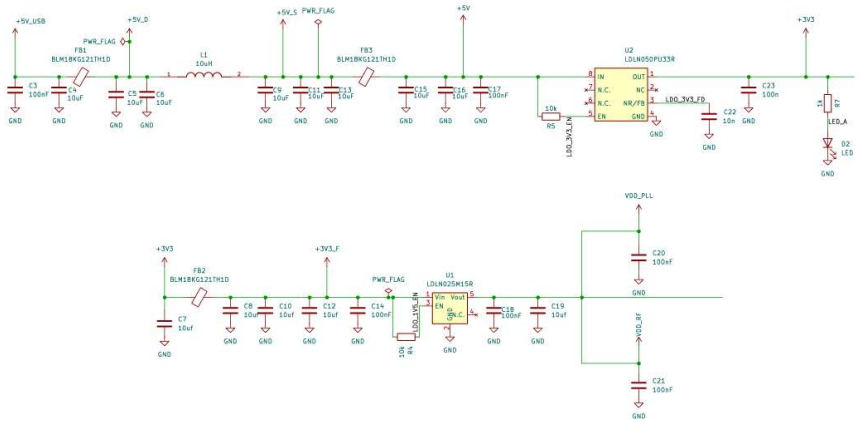

Figure 3.2: Sheet (2/3). Power supply shematic.

3.2.3 Baseband Signal Conditioning

The intermediate frequency (IF) signals extracted from the radar mixers carry the Doppler information. In Sheet 3/3, a highly accurate passive analog conditioning stage has been implemented to process these signals, in the microvolt or millivolt range,prior to analog-to-digital conversion.

Component Analysis:

- **AC Coupling Capacitors C26, C27, C32, C33 (10 nF)**: The mixers integrated into the radar exhibit a significant DC offset due to self-mixing of the local oscillator signal. These capacitors act as high-pass filters, blocking the static offset and allowing only the dynamic components generated by the target's Doppler effect to pass through. This prevents saturation of the subsequent amplification stages or the ADC.

- **Filter Capacitors C24, C25, C29, C30 (5.6 nF) and C28, C31 (150 nF)**: In conjunction with the chip's output resistors, they form analog low-pass filter networks. They act as anti-aliasing filters: they attenuate high-frequency thermal noise and out-of-band interference, limiting the passband to the useful range of Doppler signals typical of motion (from a few Hz to a few kHz).

- **Pull-up resistors R8 and R9 (10 kΩ)**: Connected to the BGT_{SELECT} and BGT_{RTSN} hardware

configuration lines. The 10 kΩ value was chosen to ensure excellent immunity to electromagnetic noise, while keeping the quiescent current consumption at just 150 μA in the event of forced logic-low switching by the host.

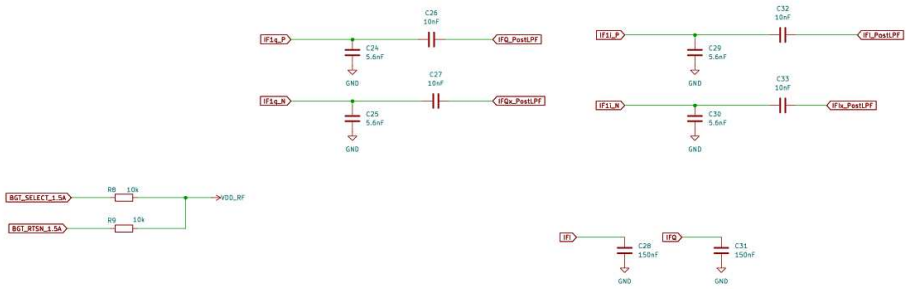

Figure 3.3: Sheet (3/3). Low Pass Filter and Pull-up Resistor schematic.

3.3 PCB Layout Design

Once the electrical schematic validation phase was complete, we proceeded with the PCB layout design. The primary objective in this phase was to preserve high-frequency signal integrity and ensure clean power delivery. The choices regarding spatial placement and routing were dictated by the need to physically isolate the noisy power conversion section from the sensitive radio-frequency section.

3.3.1 Component Placement: Top/Bottom Isolation

As shown in the 3D renderings of the board, a clear "Top/Bottom" partitioning strategy has been adopted to separate the power domains from the signal domains.

- **Top Layer**: The entire power stage, the interface connector (J1), and the filtering systems have been confined to this side. By concentrating the two LDOs (U1 and U2), the inductor (L1), and the massive ceramic capacitor banks here, we prevent high current flows and power-up transients from flowing near the RF lines. The filtering components (ferrite beads and capacitors) have been arranged in an extremely compact manner to minimize the parasitic inductance of the traces.

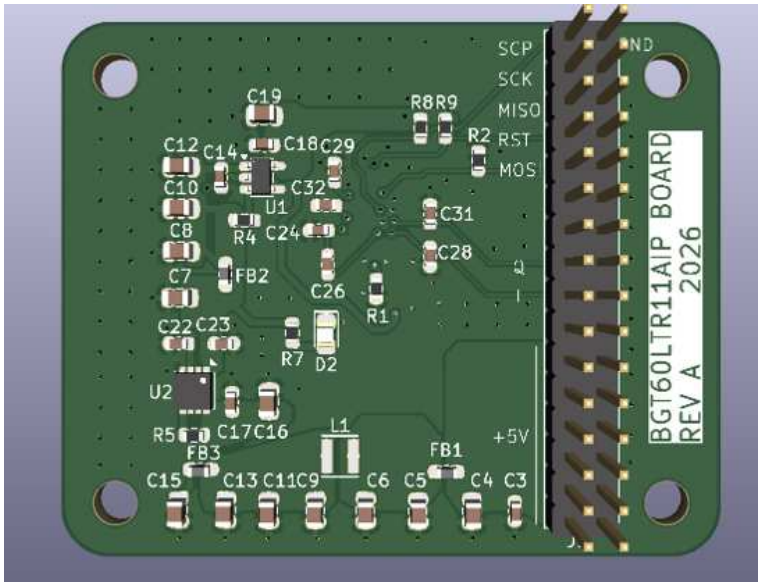

Figure 3.4: BGT60LTR11AIP Board REV A 2026 Top View

- **Bottom Layer**: The opposite side houses almost exclusively the BGT60LTR11AIP radar sensor (IC1) and its critical components. The positioning of the quartz oscillator (Y1) is of fundamental importance: it has been placed just a few millimeters from the radar's clock input pins. This extreme proximity prevents the traces from acting as antennas, avoiding the pickup of external interference that would result in clock jitter and, consequently, phase noise on the 60 GHz carrier. Furthermore, the decoupling capacitors (C1, C2, C20, C21, etc.) are placed immediately adjacent to the chip's power pins, ensuring the shortest possible path for transient currents.

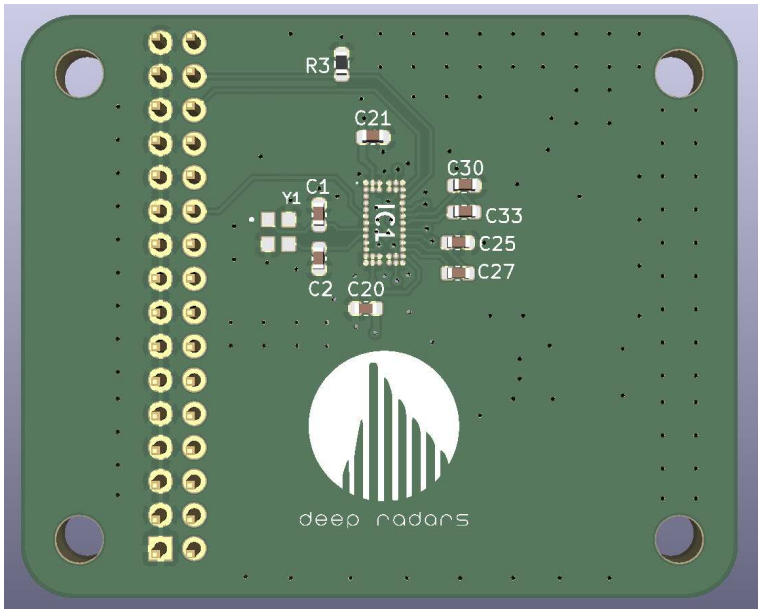

Figure 3.5: BGT60LTR11AIP Board REV A 2026 Bottom View

3.3.2 Stackup Strategy: Routing and 4-Layer Reference Planes

To manage the electrical specifications required by the 60 GHz sensor and its coexistence with the power electronics, the board was engineered on a 4-layer printed circuit board (copper layers). This choice is almost mandatory in modern RF designs to ensure signal integrity and minimize electromagnetic interference (EMI). The stackup (the PCB layering) was designed to assign specific functions to each layer:

- **External Layers (Top and Bottom)** : These are dedicated to component placement and critical signal routing. The Bottom Layer, in particular, houses the radar IC: keeping the tracks (such as those for the oscillator and integrated antennas) exclusively on an external layer avoids the use of transition vias, which would introduce lethal parasitic inductance and capacitance at radar operating frequencies. The empty areas of these layers were filled with ground polygons (GND pour).

- **Inner Layers and Power Polygons**: The two inner layers were used for power distribution (Power Delivery Network) and to provide a solid ground reference. Instead of running the power through thin traces which would have high impedance and cause voltage drops (IR drop), actual copper polygons (Power Planes) were drawn for the three system voltages: the 5V input and the regulated 3.3V and 1.5V outputs. This planar power transition offers near-zero parasitic inductance, essential for absorbing the instantaneous current transients required by the radar PLL.

- **Continuous Ground Plane and Via Stitching**: As can be clearly seen in Figures 3.7 and 3.8, the ground plane (GND) was kept as continous and uninterrupted as possible, especially in the area beneath the BGT60LTR11AIP chip. High-frequency return currents follow the path of minimum impedance, normally directly beneath the signal trace when a continuous reference plane is present to return to the source; a broken plane would create large current loops, generating electromagnetic radiation.

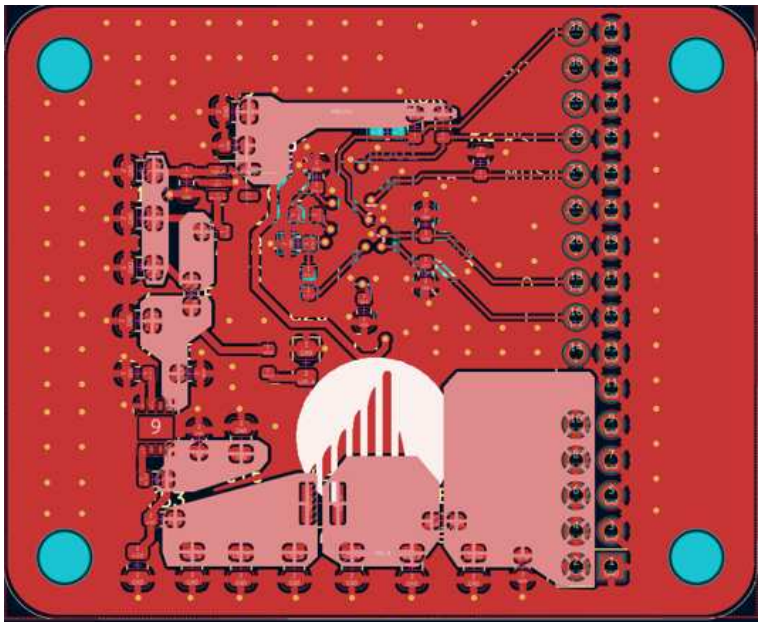

Figure 3.6: Board Power poligon

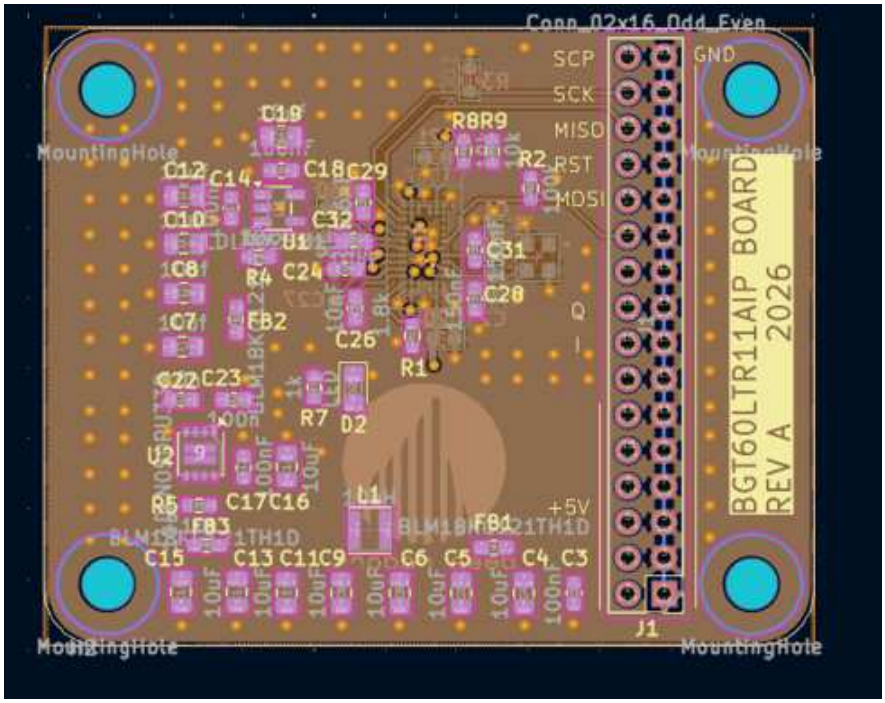

Figure 3.7: Board ground plane

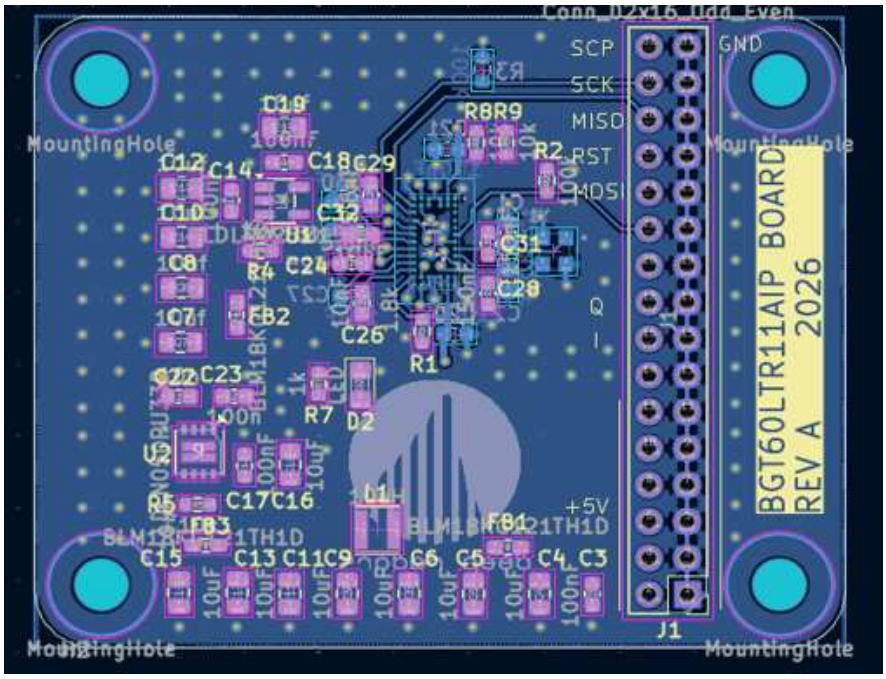

Figure 3.8: Board ground plane

To maximize this shielding effect, the top, bottom, and inner GND layers were "stitched" together using a dense array of plated holes, visible across the entire board. This technique, known as via stitching, serves two crucial purposes: it dramatically lowers the overall thermal and electrical impedance and creates a three-dimensional "Faraday cage" around the sensitive signals, effectively isolating the analog domain from the power domain.

3.4 Power supply Architecture

3.4.1 Justification for Cascaded Regulators

One of the most significant design choices visible in the layout is the adoption of two linear regulators (LDOs) in a "cascaded step-down" configuration, that is, going from the 5V input to an intermediate stage at 3.3V, and then reaching the core supply of 1.5V, rather than lowering the voltage from 5V to 1.5V with a single component. This architectural choice is dictated by two fundamental engineering reasons:

1. **Thermal Management and Power Dissipation (Thermal Management)** : Linear regulators (LDOs) dissipate the voltage difference between input and output as heat, following the ratio $P = (Vin - Vout) * I$. If a single LDO were to reduce the voltage from 5V to 1.5V (with a drop of 3.5V), and the radar were to draw, for example, 100 mA, the component would have to dissipate 0.35 Watts of heat. In such small packages, this would lead to critical overheating of the chip and surrounding PCB, degrading the thermally sensitive performance of the oscillator and radar itself. By using two stages ($5V \rightarrow 3.3V$ and $3.3V \rightarrow 1.5V$), the thermal load is evenly split between two separate ICs (U2 and U1), allowing for much safer and more efficient thermal management.

2. **Filter Multiplication and PSRR (Power Supply Rejection Ratio)**: The 5V supply from a USB port is inherently noisy. Each LDO acts as an active low-pass filter. By cascading the two regulators, their PSRR capabilities are added. The first LDO (U2) attenuates most of the USB-supply ripple, bringing the signal to a clean 3.3V; the second ultra low noise LDO (U1), already powered by a very stable source, only needs to be fine-tuned to deliver the 1.5V voltage with the extreme purity (in the microvolt range) required by the radar's RF front-end.

3.4.2 Mixed-Signal Routing: Analog and Digital Domain Isolation

A critical aspect of this board's routing stems from its inherently mixed-signal nature, characterized by the coexistence of high-speed digital signals and highly sensitive analog signals. The host microcontroller communicates with the BGT60LTR11AIP radar chip via a Serial Peripheral Interface (SPI) bus, whose clock (SCK), select (CS), and data (MOSI, MISO) signals feature very steep switching transients. These high-frequency wavefronts (with high dv/dt and di/dt values) can easily generate crosstalk by coupling capacitively or inductively with adjacent traces. If this digital noise were to reach the analog baseband traces (the In-Phase and Quadrature IF signals), it would corrupt the amplitude and phase readings, irreparably degrading the accuracy of the Doppler extraction. To avoid this risk, a strict spatial separation of the routing domains was adopted during the routing phase. As can be seen from the layout diagrams, the digital bus traces were grouped and confined to a specific area of the PCB, keeping them as short as possible between the J1 connector and the IC's digital pins, and avoiding prolonged parallelism with sensitive lines. Conversely, the analog traces were routed ensuring ample clearance from digital networks. In this context, the continuous ground plane (GND plane) located in the internal layer immediately below plays a crucial role: it confines the electromagnetic field lines beneath each trace, ensuring that the return paths of high-frequency signals remain tightly coupled to their source trace, preventing overlap and mutual interference between the digital and analog worlds.

4. Hardware Interface Design and Signal Conditioning Between Microcontroller and Radar

To evaluate the performance of the Infineon CW radar and enable data acquisition on a PC, a dedicated hardware setup was realized, supported by a custom designed 3D-printed structure. As illustrated in Figure 4.1 , the system is composed of three fundamental macro-blocks:

- **The SPI-USB Converter (Master)**: A board based on an FTDI chip (bottom right) that acts as a bridge between the PC (via USB) and the SPI serial communications protocol. This module operates at a logic voltage of 3.3V.
- **The Radar Board (Slave)**: The Infineon sensor module (top), positioned behind the dielectric lens for focusing the beam, receives and processes microwave signals. Its System-on-Chip requires 1.5V logic signals.
- **The Level Shifter (Interface)**: An intermediate circuit built on a perforated board (bottom left), which has the crucial task of ensuring safe electrical interfacing and reliable communication between the two blocks, dynamically adapting the bidirectional voltage levels between 3.3V and 1.5V. The following paragraphs will analyze in detail the need and design of the interface block (Level Shifter), which is essential for preventing hardware damage and ensuring data integrity.

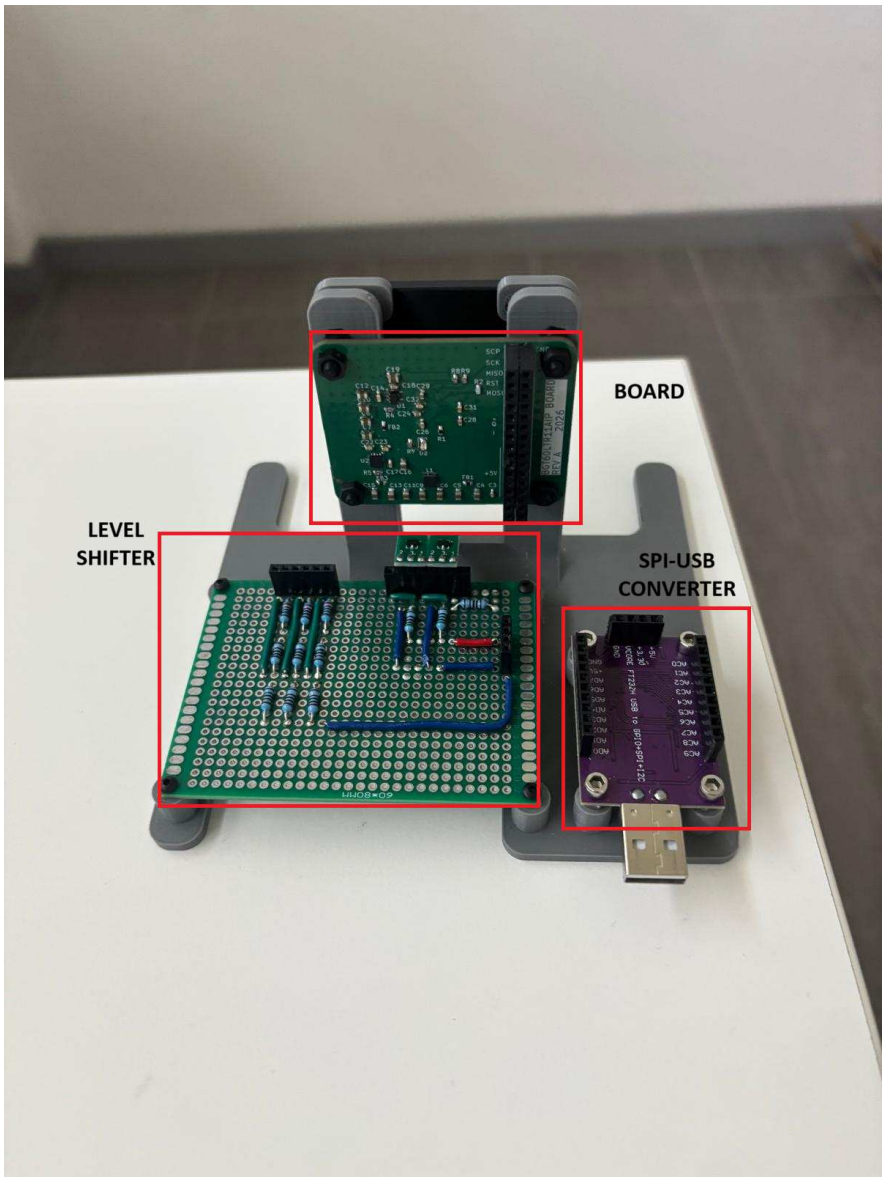

Figure 4.1: Overview of the implemented hardware setup. The system's three main modules are highlighted: the radar sensor board, the logic level shifter circuit, and the SPI-USB protocol converter.

4.1 The Importance of Level Shifting in Mixed-Voltage Architectures

The integration of electronic modules of different generations or architectures requires particular attention to the power domains. In the realized system, the USB-SPI Converter, that is responsible for communication with the host PC, it operates with standard 3.3V CMOS logic. In contrast, the Infineon radar module's System-on-Chip (SoC) uses low-power technology operating at 1.5V. Directly interfacing these two peripherals on the SPI bus presents two fundamental electrical challenges:

- **Overvoltage Stress**: Applying a 3.3V signal to an input pin designed to tolerate a maximum of 1.5V would cause irreversible damage to the gate of the receiving transistor, due to dielectric breakdown.
- **Noise Margin Incompatibility**: A radar-generated logic high (1.5V) is insufficient to reliably clear the 3.3V converter's logic high recognition threshold V_{IH}. This condition would place the line in an undefined logic region, causing erroneous readings and data corruption.

To solve these problems, we proceeded to create a "Level Shifting" circuit implemented on a dedicated stripboard, placed between the two devices. Since the SPI (Serial Peripheral Interface) protocol is asymmetric, it was necessary to differentiate the conditioning based on the direction of the signal.

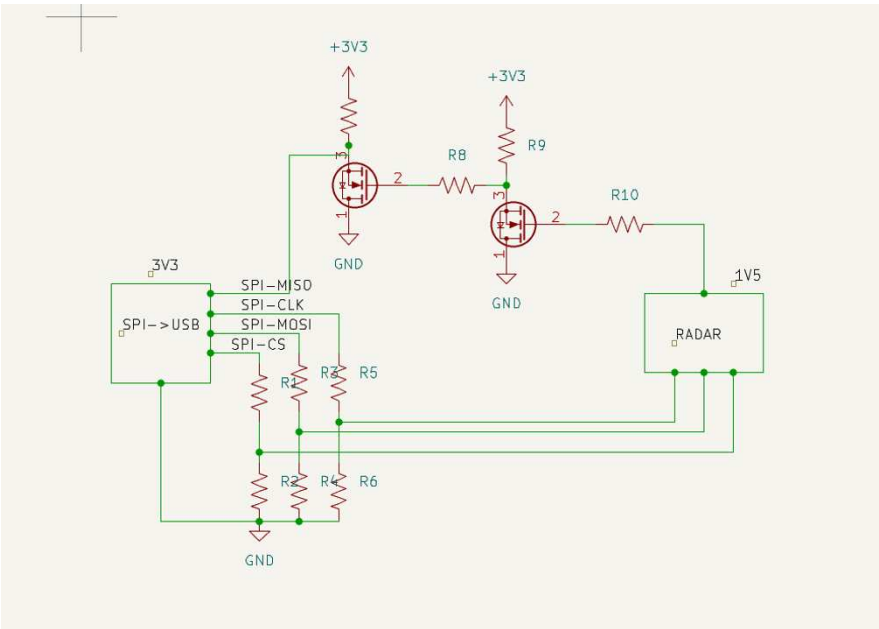

Figure 4.2: Schematic of the interfacing circuit and logic level translation (3.3V - 1.5V) between the USB-SPI converter and the radar module.

4.1.1 Step-Down Conditioning (Master-to-Slave): Resistive Dividers

The SPI bus lines controlled by the USB converter (Master) to the radar (Slave) are unidirectional: the clock signal (SPI-CLK), the data output (SPI-MOSI), and the sensor enable (SPI-CS). To lower the voltage of these signals from 3.3V to 1.5V, a network of resistive voltage dividers was chosen. This design choice ensures a robust, cost-effective, and compact solution in terms of board space. The operating principle is based on a simple application of Ohm's law, where the output voltage at the central node of the divider is given by the following equation:

$$V_{\text{out}} = V_{\text{in}} \cdot \left(\frac{R_2}{R_1 + R_2} \right) \tag{4.1}$$

By appropriately sizing the series resistor (R_1) and the ground resistor (R_2), the 3.3V voltage is attenuated to meet the radar specifications. During the design phase, choosing the resistor values required a trade-off:

- A low resistance value would lead to excessive static power dissipation absorbed by the circuit.
- An high resistance value would interact with the parasitic input capacitance of the radar pins,

creating a low-pass filter. This would result in a deterioration of the rising and falling edges (slew rate) of high-frequency signals, limiting the maximum speed of the SPI clock.

4.1.2 Step-Up (Slave-to-Master) Conditioning: The Active MOSFET Stage

The SPI-MISO (Master In Slave Out) line is controlled by the radar and has a maximum amplitude of 1.5V. To ensure reliable reading by the 3.3V converter, logic level amplification was required. Since a passive approach was impossible, an active stage with discrete components was implemented using two MOSFET transistors. The circuit is designed as a cascaded double inverting stage:

1. **First Inversion**:When the radar's MISO line switches to a logic high (1.5V), the voltage exceeds the gate-source threshold ($V_{GS(th)}$) of the first MOSFET, causing it to conduct. Its drain terminal is then pulled to logic ground (0V).

2. **Second Inversion**: This null potential is applied to the gate of the second MOSFET, forcing it into the off (open circuit) state.

3. **Signal Boost**: With the second transistor turned off, the pull-up network connected to the drain raises the node voltage up to the 3.3V reference provided by the Master.

Symmetrically, a low logic level (0V) from the radar keeps the first transistor off; the local resistor drives the gate of the second transistor high, turning it on and holding the Master's MISO line at 0V. This succession of two logic inversions returns a signal in phase with the original source, but with voltage amplitudes translated to 3.3V, thus ensuring absolute integrity of communication between the devices.

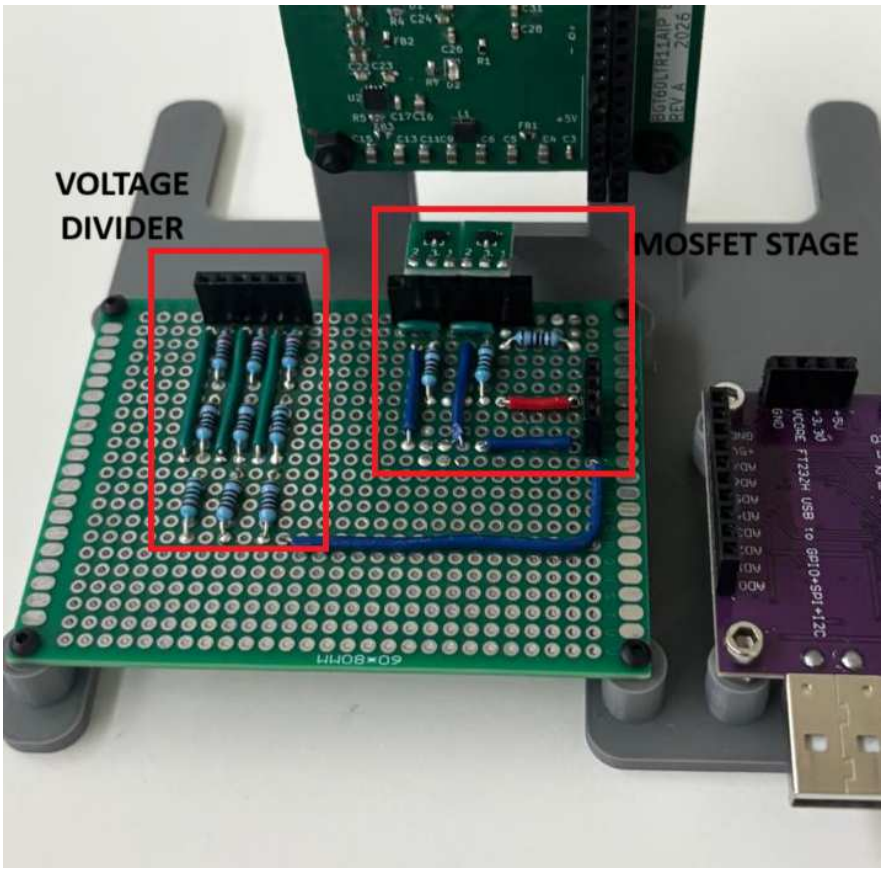

Figure 4.3: Enlargement of the conditioning circuit on a perforated board. The left panel highlights the resistor networks used to step down the signals from 3.3V to 1.5V, while the right panel shows the active MOSFET stage used to raise the MISO signal from 1.5V to 3.3V.

4.2 Beam Focusing Using a Dielectric Lens

As shown in the experimental setup in the previous subsection, the custom 3D-printed support structure serves not only to accommodate the boards but is specifically designed to precisely align a dielectric lens directly in front of the BGT60LTR11AIP radar sensor package. The introduction of this quasi-optical element in the microwave domain addresses fundamental performance limitations inherent to the bare sensor technology.

The Infineon chip adopts an AiP architecture, integrating the transmit and receive patch arrays directly into the silicon substrate. While ensuring extreme compactness and eliminating high-frequency routing losses on the PCB, these antennas exhibit a very wide radiation pattern, with a Half Power Beam Width (HPBW) of approximately 80 degrees. This large aperture translates to a structurally low directivity, as the radiated electromagnetic energy is dispersed over a vast spatial volume. This limits the sensor's maximum range and increases the reception of unwanted echoes (clutter) from lateral obstacles.

The integration of the dielectric lens effectively alters the radiation pattern, acting as a collimator. The main effects of this optomechanical integration are two:

1. **Enhanced Directivity, Gain, and Range** :By collimating the electromagnetic waves, the lens drastically narrows the main beam, resulting in a significant boost in the antenna's directivity. Since antenna gain is directly proportional to directivity, this focusing effect substantially increases both the transmit (G_T) and receive (G_R) gain parameters. According to the radar equation discussed in Chapter 2, this enhancement leads to a higher return signal power (P_R) and, consequently, a remarkable extension of the maximum detection range.

2. **Spatial Filtering and Clutter Reduction**: By narrowing the field of view, the radar achieves high spatial selectivity along the main axis of view. This minimizes multipath reflections caused by walls or adjacent objects, significantly improving the signal-to-noise ratio (SNR) for analyzing forward targets. This feature is essential for extracting micro-motion or implementing vital signs detection algorithms, where useful phase variations are millimeter-scale and highly susceptible to ambient noise.

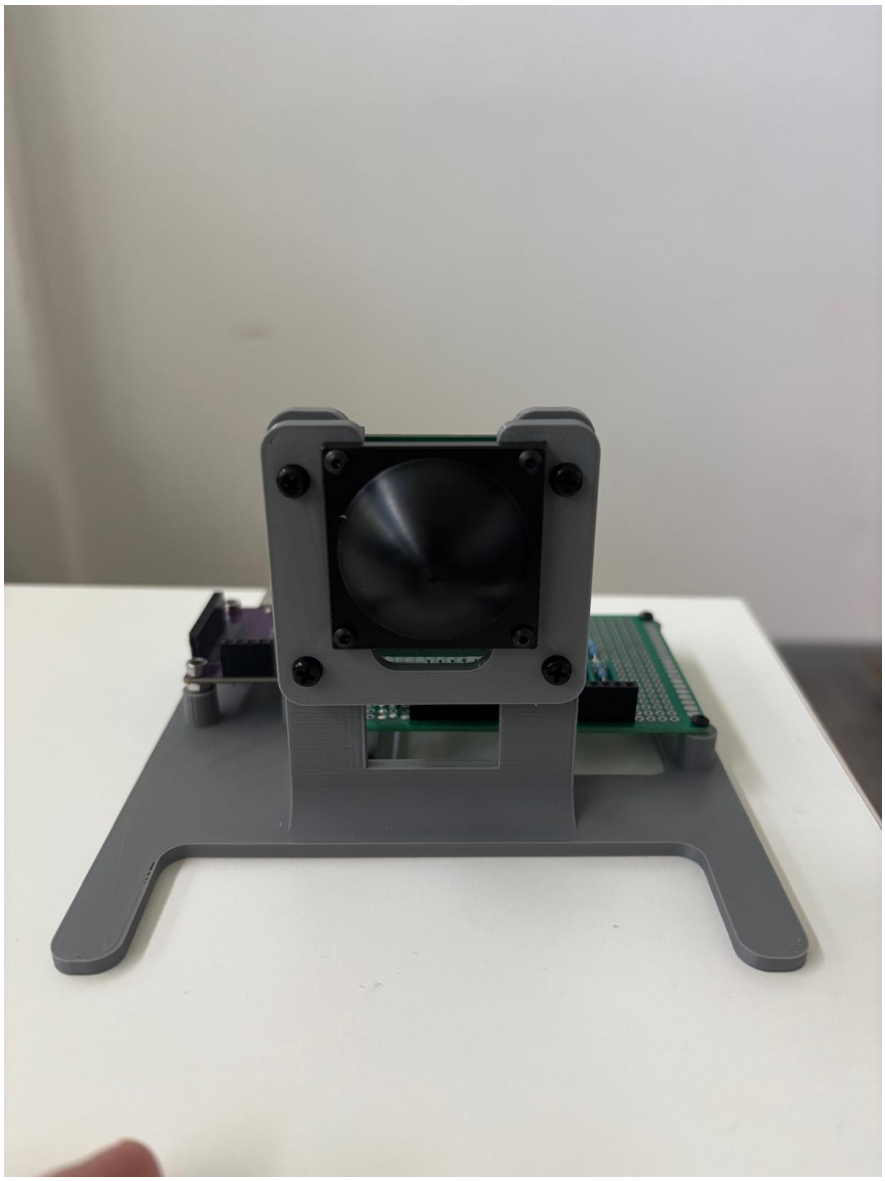

Figure 4.4: Front view of the hardware setup, highlighting the custom mount and the dielectric lens mounted in correspondence with the BGT60LTR11AIP radar chip.

In the antennas, the directivity is directly proportional to the phisycal dimension of the antenna (area or aperture) with respect the wavelenght of the signal. The antennas of the BGT60LTR11AIP chip radar are integrated on the small chip, in order to save space and eliminate signal losses on the traces, their area is microscopic. An antenna that is physically small, has not the geometric capacity to concetrate the energy in one point, so shot it in a very large cone (in our case 80 degrees). So the use of the lens resolve this problem, because the lens increase the effective area of the radiant

system. It captures the energy that the chip's tiny antenna was about to diffuse in all directions and, through refraction (just like an optical magnifying glass does with solar rays), "bends" it and realigns it along a single axis. As result, the main radiation lobe becomes much narrower. By reducing this aperture angle, the directivity antenna increases. Concentrating the beam in a single forward direction not only increases the maximum detection range, but also acts as a spatial filter. It ignores lateral clutter, maximizing the Signal-to-Noise Ratio (SNR) for the target in front of the radar.

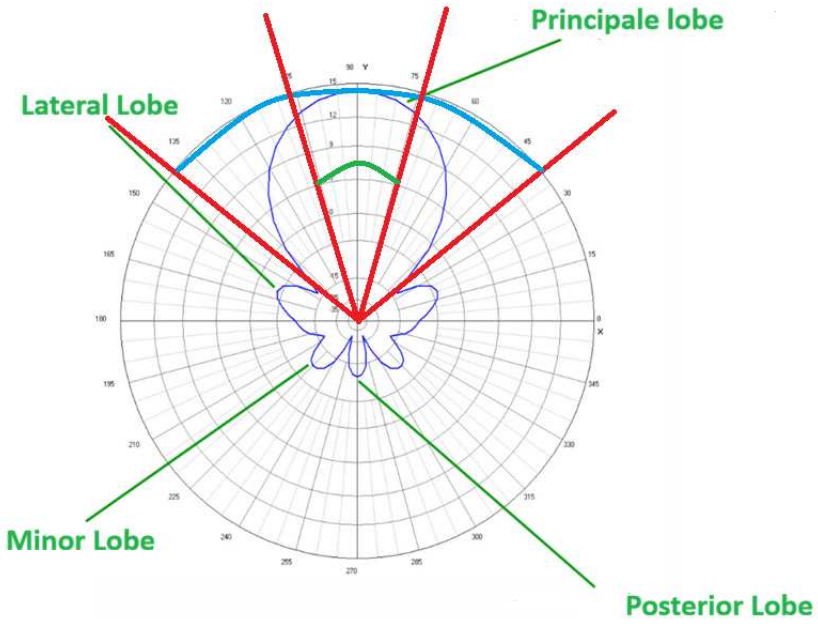

Figure 4.5: Representation of the different emission lobes of an antenna (main, side, minor, and rear). The red lines and colored arcs conceptually illustrate the effect of the dielectric lens: reducing the aperture angle (transition from the blue arc to the green arc) narrows the main lobe, increasing directivity and reducing exposure to lateral clutter.

4.3 Experimental Results

In order to validate the working of the developed board and the radar sensor, we test it by realizing a precise setup. The board is placed in front of a mechanical target set to move periodically back and forth along the sensor's visual axis at a constant speed. The base Band analog signals (BBI, Baseband In-Phase, and BBQ Baseband Quadrature) extracted by the radar, were acquired and tracked to analyze the motion response.

4.3.1 Signal Analisys in Time Domain (I and Q)

The Figure 5.6 shows the time evolution of the two signals I and Q representing a specific fragment of the acquisition where the target moves at a constant velocity When the 60 GHz continuous wave emitted by the radar hits the moving target, the reflected wave undergoes a frequency shift known as the Doppler effect. The chip's internal demodulator "subtracts" the original frequency from the received one, returning only this difference as the output. The result is two low-frequency sine waves. Observing the graph, we can draw some important conclusions:

- **Constant Velocity**: The fact that the waves have a constant frequency (i.e., distance between peaks) over time confirms that the target was moving at a constant speed.
- **Directional phase shift**: The I and Q signal are approximately 90 degrees out of phase with each other (note that when one is at its maximum, the other passes through zero). This phase shift is designed into the radar architecture to allow the system to determine the target's direction. If the I signal leads the Q, the target is approaching; if the opposite is true, it is receding.

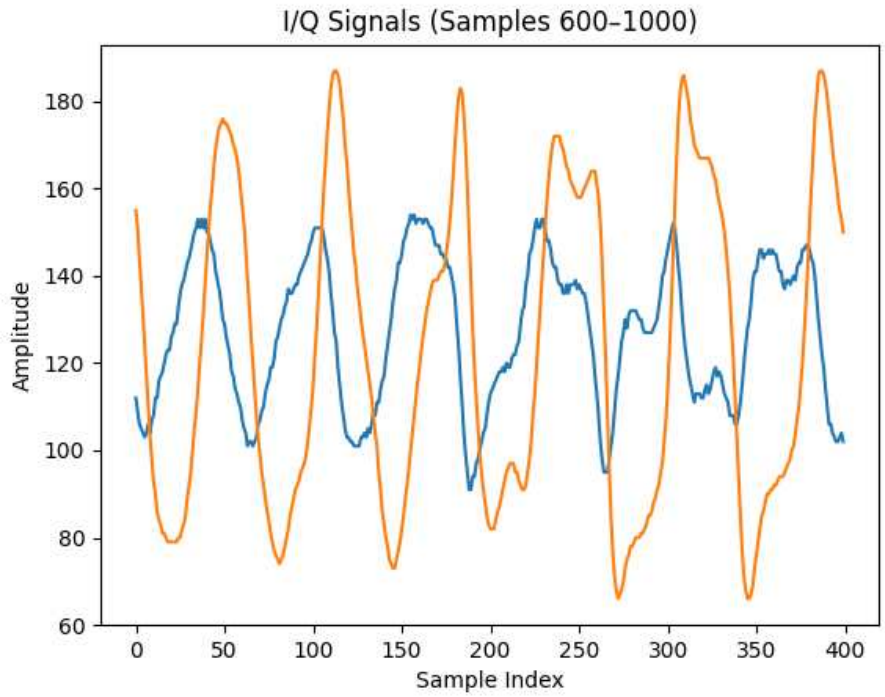

Figure 4.6: I and Q signals results.

4.3.2 Constellation Graph Analysis

The second graph shows the so-called "constellation," where the horizontal axis represents the instantaneous value of the I signal and the vertical axis represents the Q signal. The explanation for the formation of a sort of circle is that the I signal is proportional to the mathematical function cosine, while the Q signal is proportional to the sine. If we plot a point on a Cartesian plane with the X coordinate of a cosine and the Y coordinate of a sine, over time this point will trace a perfectly circular trajectory. However, observing the graph obtained by real data, we can see that the shape is not a perfect circle, but resembles an ellipse. This phenomenon is known as **I/Q Imbalance** and this is not a defect of the board but is a normal behavior of the radar. We have:

- **Amplitube Imbalance**: two internal amplifiers (VGA) do not have exactly the same gain, so one wave is slightly "higher" than the other (in this case the Q axis is wider than the I axis).
- **Phase Imbalance**: The phase shift generated by the internal oscillator is never mathematically perfect at 90 degrees.

- **DC Offset**: Electronic circuits always add a very small residual DC voltage, which moves the center of the circle away from the coordinates (0,0).

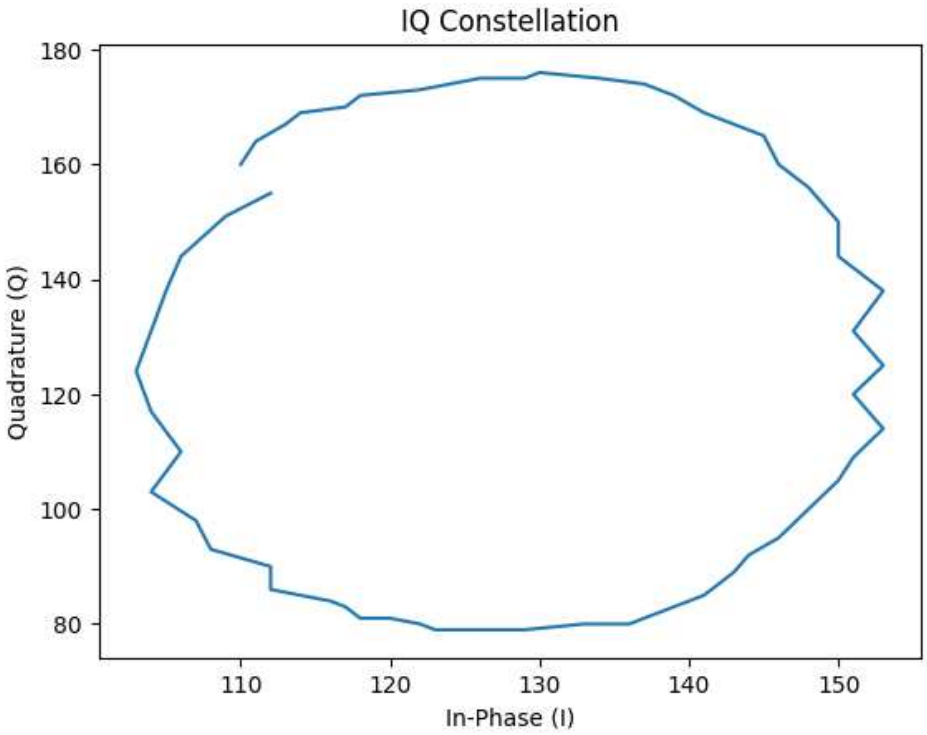

Figure 4.7: Constellation plot.

4.4 Phase Extraction and Phase Unwrapping

To measure target motion, it is not sufficient to observe only the amplitude of the demodulated signals; the signal phase must also be extracted. As discussed previously, the quadrature architecture provides two orthogonal baseband signal: the I signal, that is proportional to a cosine function and the Q Signal that is proportional to a sin function. In this experimental setup, these signals were acquired with a sampling frequency of 1 kHz over a total duration of 20 seconds, providing a dataset with high temporal resolution suitable for analyzing micro-movements. Utilizing this trigonometric relation, the istantaneous phase $\phi(t)$ of the reflected signal can be calculated point by point by calculating the arctangent of the ratio between the 2 signals:

$$\phi(t) = \arctan\left(\frac{Q(t)}{I(t)}\right) \tag{4.2}$$

Concerning to the software, this operation is tipically implemented by the function $atan2(Q, I)$, which takes into account the signs of both operands to correctly map the result to all four quadrants, returning a phase value limited in the mathematical range between $-\pi$ and $+\pi$. However, the direct use of this formula introduce a non-negligible problem. When the displacement of the target is sufficiently large to cause a phase variation larger than a π, the value calculated by the arctangent undergoes a discontinuity, creating a sawtooth pattern and jumping abruptly from $+\pi$ to $-\pi$ or viceversa, which does not reflect the real physical and continuous movement of the object. To reconstruct the true displacement of the target, it is necessary to apply a Phase Unwrapping algorithm. This algorithm analyzes the sequence of phase samples and detects abrupt jumps. When the phase difference between two consecutive samples exceeds a certain threshold (typically close to π). The software compensates for this discontinuity by adding or subtracting an offset equal to 2π. The end result of this algorithmic compensation is clearly visible in Figure 4.8, which shows the continuous unwrapped phase signal ϕ(t) over a 20 second observation window. The reconstructed signal is directly and linearly proportional to the radial displacement $\Delta R(t)$ of the target relative to the radar, according to the fundamental mathematical relationship:

$$\Delta R = \frac{\lambda}{4\pi}\phi(t) \tag{4.3}$$

where λ is the 5 millimeter wavelength corresponding to the 60 GHz carrier frequency. By observing the time domain waveform in Figure 4.8, we can extract critical physical information

about the target's motion:

- **Periodic Displacement**: The regular, sinusoidal-like oscillation confirms that the mechanical target is performing a continuous back-and-forth movement along the sensor's line of sight.
- **Amplitude of Oscillation**: The peak-to-peak phase variation spans approximately 100 rad that corresponds to about 40 mm peak-to-peak displacement.
- **Motion direction and reversal**: The positive slopes of the curve represent the phases where the target is moving in one direction, while the negative slopes indicate the exact moments of motion reversal and receding velocity.

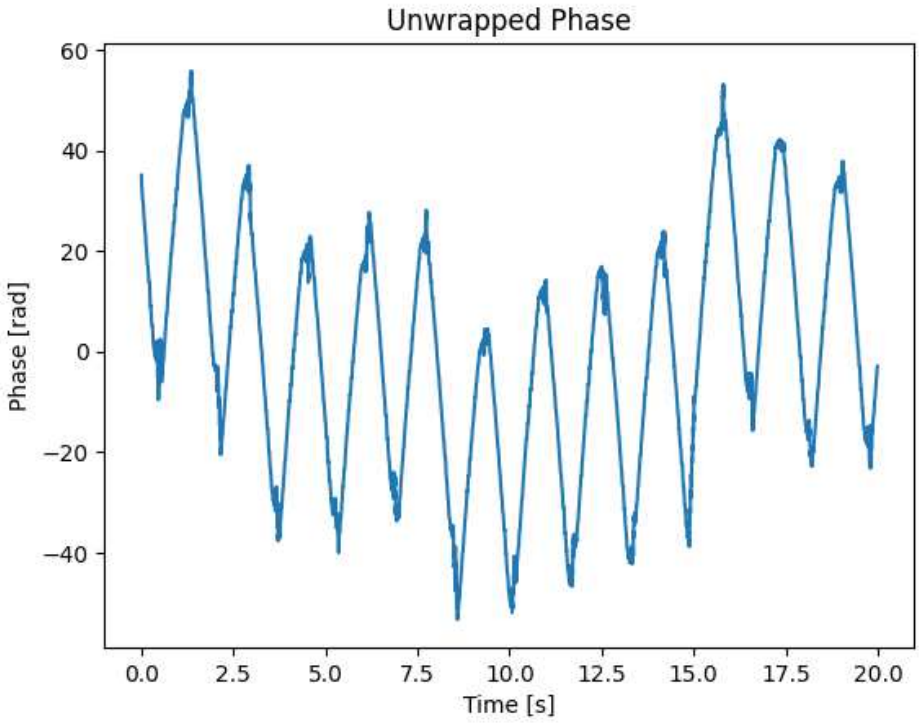

Figure 4.8: Unwrapped Phase plot.

4.5 Oscillation Frequency Estimation

Once the continuous phase signal has been obtained and the discontinuities have been removed by the phase unwrapping, the extracted information represents the radial temporal displacement of the target with respect to the sensor. In the case of micro-movements, this temporal signal is the result of the superposition of multiple oscillatory components at different frequencies, often obscured by background noise or environmental vibrations. To quantitatively isolate these frequencies and estimate the periodic behavior of the oscillation, a transition from the time domain to the frequency domain is necessary. This process is implemented by applying the FFT to the unwrapped phase signal.

Before applying the FFT algorithm, to avoid spectral distortions, the time sequence of the data is multiplied by an analytical windowing function. This windowing operation aims to gradually attenuate the signal near the edges of the observation window, eliminating artificial discontinuities due to signal truncation over time. This drastically reduces the phenomenon of spectral leakage, which would otherwise create secondary lobes in the spectrum that could mask the weaker frequency components. Subsequently, the FFT of the windowed signal is calculated and the amplitude spectrum (modulus of the transform) is extracted. In the frequency domain, each regular periodic oscillation present in time translates into a well-defined spectral peak, whose coordinate on the x-axis indicates the exact frequency of the oscillation expressed in hertz.

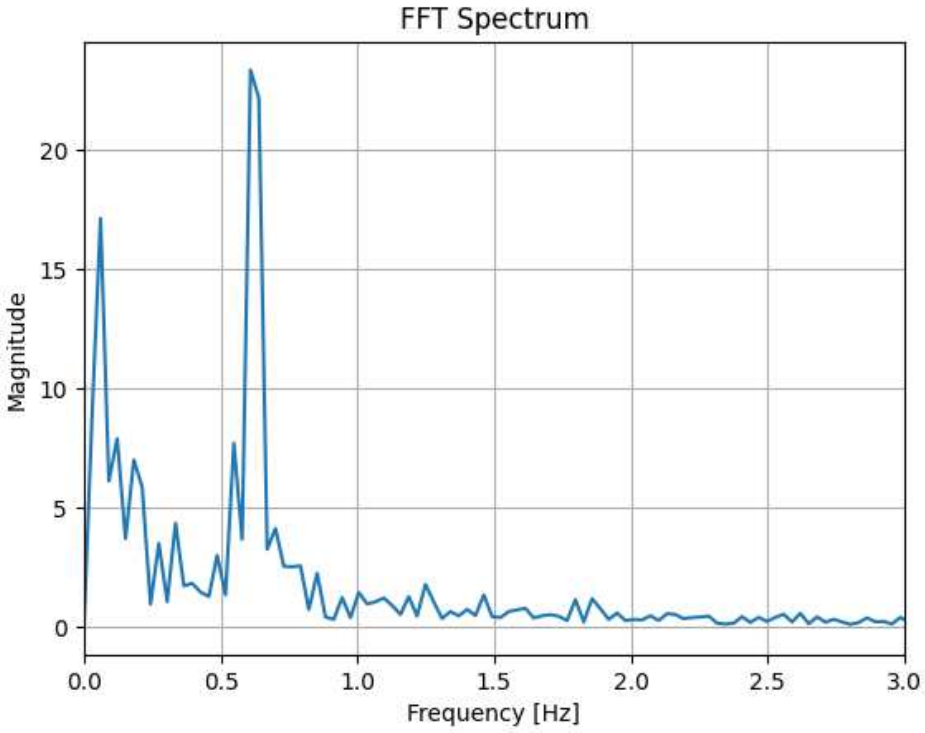

Figure 4.9: FFT Spectrum plot.

Analyzing the spectrum in Figure 4.9 yields the following key findings:

- **Dominant Oscillation Frequency:** The spectrum exhibits a sharp, highly prominent peak located at $f \approx 0.6$ Hz. This spectral component represents the fundamental frequency of the target's oscillation.
- **Experimental Validation:** This mathematical estimation precisely matches the actual physical frequency that was set on the mechanical target during the laboratory experiment (corresponding to 0.6 cycles per second, or 36 complete back-and-forth oscillations per minute).
- **Low-Frequency Noise Rejection:** The smaller amplitude variations observed below 0.3 Hz can be attributed to minor environmental vibrations, thermal drift, or residual DC offset anomalies. However, the high Signal-to-Noise Ratio (SNR) achieved by the system ensures that the true Doppler frequency stands out unmistakably.

This result successfully validates the entire signal conditioning chain and processing pipeline. It proves that the custom BGT60LTR11AIP board, combined with phase unwrapping and FFT

analysis, is fully capable of extracting sub-hertz micro-movements and frequencies with a clear spectral peak at the imposed oscillation frequency.

4.6 Prototyping Cost Analysis

One of the main goals of this project was to create an integrated custom board while keeping the costs compatible with future scaling. The total budget to build the entire setup including the radar board, interface circuits and mechanical supports was around €190. The major expense is due to the fabrication of the 4 layer board. However, because an on-chip radar was used, the board can be developed with a low-cost FR4 material. As regard the electronics components, is very interesting to note how the main technological part of the system the Infineon chip radar BGT60LTR11AIP has a low cost, approximately €7/8. It is important to underline that this €190 represents the cost of the prototype, where each single component is purchased individually.
The relative costs for each component used to realize the board are shown in Table 4.1.

Table 4.1: Bill of Materials (BOM) of the prototype.

Component	**Description**	**Quantity**	**Unit Price (€)**
BGT60LTR11AIP	Radar Sensor 60GHz	5	8.00
LDLN025M15R	LDO Regulator 1.5V	5	1.20
FH3840024Z	Crystal Oscillator	5	0.70
CL10B154KO8NNNC	150nF Capacitor	10	0.05
C0603C120F5HAC	12pF Capacitor	10	0.15
0603ZC562KAT2A	5.6nF Capacitor	20	0.10
MCT06030C1003FP500	100kΩ Resistor	10	0.08
CRCW06031K80FKEC	1.8kΩ Resistor	5	0.08

Despite a total setup cost of about €190 (which includes a shipping of approximately €50) for five prototypes, the electronics components are extremely low cost. This data highlights the enormous scalability potential of the platform: in an industrial production scenario, where PCB manufacturing costs (currently high for small batch production), the cost of the entire board could drop dramatically. As a preliminary estimation, considering the raw component cost, for a single prototype of about €10, and considering that the fixed costs scale down vertically, the overall unit cost, including automated assembly and PCB fabrication at scale, could settle at around €10–15 per unit.

5. Conclusion and Future Development

This thesis documented the entire design and validation path of an embedded system based on the Infineon chip radar BGT60LTR11AIP. Starting from the theoretical foundations of radar technology, this project has successfully transformed abstract mathematical models into a fully functioning physical prototype. Using the AiP technology, a 4-layer PCB was designed and the board design ensured signal integrity through a robust power network. To establish a reliable communication between the radar architecture (1.5V) and the microcontroller (3.3V), a level shifter was designed and the usage of a dielectric lens has proven to be an effective solution for narrowing the radar's field of view, increasing its directivity and reducing lateral clutter and lateral echoes.

As regard the experimental results, the system has acquired successfully the baseband signals, I and Q, generated by a moving target. Through processing of the acquired data, it has been demonstrated that, despite the intrinsic hardware imperfections of the sensor such as I/Q imbalance, the application of the mathematical techniques specifically the Phase Unwrapping algorithm and Fast Fourier Transform allows for the accurate extraction of micro-displacements and oscillation frequencies.

Now that a stable, economical and reliable hardware base has been built, future developments of this project will be able to range across different fronts, in perfect line with the needs of industrial automation and the IoT. From an architectural point of view, the next step will consist of integrating the level shifter and a microcontroller directly on the board, and this will remove the necessity to have external interface modules, further reducing the dimensions and transforming the system into a completely autonomous sensing system.

Bibliography

[1] Maurizio Di Paolo Emilio. *La tecnologia Radar*. Elettronica Open Source. 2017. URL: https://it.emcelettronica.com/la-tecnologia-radar.

[2] Elia Vignoli, Pasquale Di Viesti, and Giorgio Matteo Vitetta. "A Deterministic Method for Contactless Monitoring of Vital Signs Using Multiple FMCW Radars in the 24 GHz Band". In: *IEEE Access* 13 (2025), pp. 27868–27892. URL: https://ieeexplore.ieee.org/document/10879000.

[3] G. Paterniani et al. "Radar-Based Monitoring of Vital Signs: A Tutorial Overview". In: *Proceedings of the IEEE* 111.3 (2023), pp. 277–317. URL: https://ieeexplore.ieee.org/document/10049295.

[4] Christian Wolff. "Principi di base del Radar: Risoluzione in distanza". In: *Radar Tutorial* Sezione 02.07 (2026), p. 1. URL: https://www.radartutorial.eu/02.basics/rp07.it.html.

[5] Manmohan Sharma. "An Impulse-Radio UWB signal containing short pulses with a low duty cycle". In: *ResearchGate* Fig. 13 (2015), p. 1. URL: https://www.researchgate.net/figure/An-Impulse-Radio-UWB-signal-containing-short-pulses-with-a-low-duty-cycle-Here-i-i_fig13_319650834.

[6] Texas Instruments. *The fundamentals of millimeter wave radar sensors (Rev. A)*. 2017. URL: https://www.ti.com/lit/wp/spyy005a/spyy005a.pdf.

[7] Infineon Technologies. *BGT60LTR11AIP EBG shield - User Manual*. 2023. URL: https://www.infineon.com/assets/row/public/documents/24/44/infineon-ug133733-bgt60ltr11aip-ebg-shield-usermanual-en.pdf.

[8] Infineon Technologies. *BGT60LTR11SAIP Datasheet*. 2022. URL: https://www.infineon.com/assets/row/public/documents/24/49/infineon-bgt60ltr11saip-datasheet-en.pdf.

[9] Diodes Incorporated. “FH Series 2.5x2.0 Seam Sealed Crystal Datasheet”. In: *Diodes Incorporated Datasheets* Rev. F (2018), pp. 1–4. URL: https://www.diodes.com/assets/Datasheets/FH.pdf.

[10] STMicroelectronics. “LDLN025: 250 mA ultra-low noise LDO Datasheet”. In: *STMicroelectronics Datasheets* DM00312779 (2020), pp. 1–35. URL: https://www.st.com/resource/en/datasheet/dm00312779.pdf.

[11] STMicroelectronics. “LDLN050: 500 mA, high performance low dropout linear regulator Datasheet”. In: *STMicroelectronics Datasheets* DM00557249 (2021), pp. 1–33. URL: https://www.st.com/content/ccc/resource/technical/document/datasheet/group3/6d/d0/b4/42/e7/d5/40/f6/DM00557249/files/DM00557249.pdf/jcr:content/translations/en.DM00557249.pdf.